UNIVERSITY OF CALIFORNIA, SAN DIEGO

Noninvasive Cardioneural Signal Extraction

A thesis submitted in partial satisfaction of the
requirements for the degree
Master of Science

in

Computer Science

by

Amirali Shayan Arani

Committee in charge:

Professor Chung-Kuan Cheng, Chair
Professor Andrew Kahng
Professor Garrison Cottrell

2008

The thesis of Amirali Shayan Arani is approved and is acceptable in quality and form for publication on microfilm and electronically:

_____

_____
Co-Chair

_____
Chair

University of California, San Diego

2008

TABLE OF CONTENTS

LIST OF FIGURES

LIST OF TABLES

ACKNOWLEDGEMENTS

I owe many thanks to my advisor Professor Chung-Kuan Cheng for his endless guidance and support over the course of my research. I would like to thank my collaborators Dr. Peng-Sheng Chen and Dr. Shien-Fong Lin from Krannert Institute of Cardiology, Indiana University whom this work was inspired from. For most of this work I benefit from the help and suggestions of my colleague Yi Zhu from UCSD VLSI lab. I would also appreciate the suggestions from my collaborators: the researchers from Swartz Center for Computational Neuroscience at UCSD, Tzyy-Ping Jung, Jeng-Ren Duann, and Scott Makeig.

ABSTRACT OF THE THESIS

Noninvasive Cardioneural Signal Extraction

by

Amirali Shayan Arani
Master of Science in Computer Science

University of California San Diego, 2008

Professor Chung-Kuan Cheng, Chair

Heart activities are governed by the sympathetic and parasympathetic nervous system. Changes in these neural signals influence the development of arrhythmias, including ventricular tachyarrhythmias that often progress to sudden cardiac death (SDC). A simultaneous study of the cardioneural signals with the electrical heart activity can elucidate the mechanism of abnormal heart activity. In this work, we identify the locations to detect cardioneural signals. We first perform a high density electrode measurement to explore the cardioneural signals. We then focus on selected locations for longer period measurement. We monitor the changes in the heart rate following each sympathetic or vagal nerve activity. The neural signals are extracted from ECG by applying independent component analysis. The work provides a promising approach for studying the association of cardioneural signals with electrical heart activity.

1

Introduction

According to American Heart Association heart diseases are America's number one killer. Cardioneural signal influence heart activities and rhythms. Damage to nerves extrinsic to the heart, such as the stellate ganglia, as well as to intrinsic cardiac nerves from diseases that may affect nerves primarily, such as viral infections, or secondarily, from the disease that cause cardiac damage, may produce cardio neuropathy. Also, the nerve fiber density and regional sympathetic hyperinnervation in the ventricles is correlated with the occurrence of spontaneous ventricular tachyarrythmia or Sudden Cardiac Death.

In this work we proposed a comprehensive study for exploring and analyzing cardioneural signal to track, monitor and potentially prevent heart arrhythmias. In our current study, we explored the cardioneural signal from noninvasive measurements. Previously, *Jung* et al.[19] performed an invasive nerve study for monitoring the circadiane nerve activities in ambulatory dogs. Their study results motivated us, to develop an original research for exploring the cardioneural signal on human subjects. Hence, we performed both high density and portable noninvasive measurements to extract the cardioneural signal. We tried different combinations of the activities and location to probe the cardioneural signal based on the heart rate variation. We applied ICA algorithm to decompose the cardioneural signal from mixture of ECG measurements. The qualitative promising results demonstrate the feasibility of this direction.

First, we develop set of high density Electrocardiogram (ECG) measure-

ments with around 100 electrodes for a comprehensive study of the ECG signal. Then we applied Independent Component Analysis algorithm as a blind source decomposition method for decomposing original ECG temporal and spatial sources. We analyzed the back projection of each source and its corresponding dipole vector on the body surface potential map to localize failure in the heart activity. Since 100 channels were redundant for the separation, we derived a methodology for the minimum possible electrode number and locations. We proposed the method for localizing each ECG source component dipole vector that can be used to track the activity of each source during the time and space domain. This approach facilitates the feasibility of the ICA study on the patients with moderate spatial resolution, since it requires significantly fewer leads for recording and easier diagnosis setup.

Next, we explored cardioneural signal which is used for tracking and monitoring heart arrhythmias. We performed both high density and portable noninvasive measurements on human subject to localize the cardioneural signal. We extract cardioneural signal using ICA. Our method and experimental results show a promising method to extract the neural signals from ECG sources. We localized the cardioneural signals based on the changes in the heart rate and the symmetric SGNA. We applied ICA to decompose the cardioneural signals from the ECG mixture.

In the next chapter, we will discuss high density ECG experiment and the source decomposition using ICA. In chapter 3m the spatial density reduction of the ECG measurement will be discussed. We will introduce the high density noninvasive cardioneural signal extraction procedure and methodology in chapter 4. The portable cardioneural extraction using Holter will be introduced in chapter 5. Finally, in chapter 6 we will discuss the future direction of this promising research.

2

Analyzing High-Density ECG Signals

The analysis of electrocardiographic (ECG) signals is of fundamental importance for cardiac diagnosis. Conventional ECG recordings, however, use a limited number of channels (12) that each records a mixture of activities generated in different parts of the heart. Therefore, direct observation of the ECG signals collected on the body surface is likely an inefficient way to study and diagnose cardiac abnormalities. This study describes new experimental and analytical methods to capture more meaningful ECG component signals, each representing more directly a physical cardiac source. This study first describes a simply applied method for collecting high-density ECG signals. The recorded signals are then separated by independent component analysis (ICA) to obtain spatially fixed and temporally independent component activations. Results from five subjects show that P, QRS and T waves can be clearly separated from the recordings, suggesting ICA might be an effective and useful tool for high-density ECG analysis, interpretation and diagnosis. This is a promising approach and is able to be extended to perform more sophisticated heart simulations.

2.1 High Density ECG measurement

It is no doubt of importance for doctors to identify how the cardiac patient's heart is working. Electrocardiographic (ECG) recording provides a way to estimate cardiac functions by measuring the electrical fields it generates. Although ECG can record noninvasive measurements of heart activity, because of the confounds created by mixing of volume-conducted signals at the body-surface electrodes, a healthy subject could have an abnormal appearing heart rhythm and a known cardiac-impaired subject, a normal heart rhythm [2]. Thus, diagnoses based on visual observation of recorded ECG signals may not be accurate. To achieve a better understanding of how the heart works requires that the recorded body-surface signals be spatially filtered to reveal their underlying cardiac source signals, better allowing the doctor to understand how each source contributes to the cardiac cycle.

In this section, we introduce our approach to make use of Independent Component Analysis (ICA) techniques to analyze electronic heart signals recorded using high-density montages. ICA refers to a family of related algorithms that performs blind source separation when statistical independence are taken into account[17]. Although ICA and the similar technique PCA (Principal Component Analysis) has been applied to analyze atrial activities in ECG [33][9][8], only conventional 12-lead ECG data were used therefore the number of sources that could be separated was limited to 12. On the other hand, multiple channel recordings were used by other researchers, such as [32][27][28], but they did not study the different independent components embedded in the recorded heart waves by using high density electrodes. The major contributions of the high density analysis work are as follows:

1. We design the experiments to record high-density (98 channels) from the body surface of subjects. The signals have high quality and are stable when subjects do various activities. This enables us to apply ICA on the recorded data, as multi-channel recording is necessary for ICA to separate underlying components.

2. We employ the gradient ascent ICA algorithm to separate the components in the recorded mixed signals. For all the 5 subjects, we are able to separate the P-wave, QRS complex and T-wave, which shows that this method is an effective way to identify the different sources of ECG signals.

3. We develop back-projection algorithm to plot the potential map of each separated component, and devise a simulated annealing algorithm to estimate the dipole of each component. The results demonstrate that different components possess different properties, which indicates that these approaches are promising to locating the underlying problems of human hearts compared to traditional ECG analysis.

The rest of the chapter is organized as follows: in the next section, we will present the analysis methods used in our study, which includes independent component analysis, back projection, and dipole estimation algorithms. Section 3 will describe the procedure of our experiments. The experimental results and analysis will be shown in Section 4.

2.2 Analysis Methods

2.2.1 Independent Component Analysis

Our methods are based on the theory of ICA, which was originally proposed to solve the blind source separation problem [10]. In his pioneering contribution, Comon defined the mathematical framework for ICA, setting the foundations for the development of further research on the topic. Research efforts in ICA were small scale until the mid 1990s, when it gained more attraction and popularity based on Bell and Sejnowski's infomax approach [17]. Makeig et al. first applied ICA to analyze electroencephalographic (EEG) data [29]. Jung, Makeig, Sejnowski, and their colleagues applied the ICA technique to several different types of biomedical signals including ECG, EEG, MEG (the magnetic counterpart to EEG), and functional magnetic resonance imaging (fMRI) scans [22][23].

Early ECG applications focused mainly on two directions. De Lathauwer *et al.* first applied ICA to separate the fetal ECG from maternal body-surface ECG recordings [24][25], successfully addressing a longstanding problem dating back to work in [42]. More detailed results were given by [41] and [35]. The use of ICA to remove artifacts from ECG recordings were noted by [43][1][13]. ICA was also used to remove ECG artifacts from both animal [40] and human [21] recordings. Park et al. used ICA to decompose ECG signals [31]. However, they only made use of the conventional 12-lead ECG signal from which only 10 channels of recorded data were available for analysis. And they did not instruct subjects to perform multiple activities. ICA separated components accounting for the QRS complex from those accounting for the P-wave and T-wave. But they were unable to further separate P-wave from T-wave; Here, more elaborate methods are designed to collect high-density ECG signals and used ICA to separate the underlying heart activities. The ICA concept and algorithm are introduced as follows.

N source signals $s = \{s_1(t), \ldots, s_N(t)\}$, linearly mixed by multiplying a mixing matrix A, produce N mixture signals $x = \{x_1(t), \ldots, x_N(t)\} = As$. Given the signal mixtures x, we would like to recover a version, $u = Wx$, of the original sources, s, identical to the original save for scaling and permutation, by finding a square unmixing matrix, W. The key assumption used in ICA to solve this problem is that the source signals are as statistically independent as possible during the time course of the recordings. By definition, statistical independence means the joint probability density function (pdf) of the output sources can be factorized to the product of the marginal pdfs of each source:

$$p(u) = \prod_{i=1}^{N} p_i(u_i) \tag{2.1}$$

There are quite a few ICA algorithms, such as Hyvarien's FastICA and Cardoso's fourth-order algorithm JADE[7][6]. They have similar performance when generally compared. However, when applied to actual data sets, they may produce difference solutions and the significance are hard to measure. The review papers [26] , [16] compared various ICA algorithms and their interrelationships. Here we employ the gradient ascent algorithm implemented by Makeig *et al.* [29] , which

is based on the infomax ICA algorithm that has been proven to be effective in analyzing biomedical signals[23]. In the below we briefly sketch the infomax ICA algorithm and the gradient ascent approach.

The objective of the infomax ICA algorithm is to minimize redundancy between the outputs, which is the following mutual information

$$I(u) = \int p(u) \log \frac{p(u)}{\prod_{i=1}^{N} p_i(u_i)} du \tag{2.2}$$

This redundancy measure has value 0 when the pdf $p(u)$ can be decomposed as in Equation (1), and is a difficult function to minimize directly. Therefore the infomax algorithm relates this function to the joint entropy, $H(g(u))$, where $g(u)$ is the cumulative density function (cdf):

$$I(u) = -H(g(u)) + E\left[\sum_{i=1}^{N} \log \frac{|g_i'(u_i)|}{p_i(u_i)}\right] \tag{2.3}$$

If the absolute values of the slopes of the cdfs, $|g_i'(u_i)|$ are the same as the independent component pdfs,$p_i(u_i)$ then maximizing the joint entropy of the $g(u)$ vector will be equivalent to minimizing the redundancy in the u vector.

Based on this idea, the unmixing matrix W can be updated iteratively using the following equation[29]:

$$\Delta W = \epsilon \frac{\partial H(g(u))}{\partial W} W^T W = \epsilon (I + \hat{y} u^T) W \tag{2.4}$$

where ϵ is the learning rate and vector $\hat{y}$ has the elements $\hat{y}_i = (\frac{\partial}{\partial u_i}) \log(\frac{\partial g_i(u_i)}{\partial u_i})$. The $(W^T W)$ "natural gradient" term in the update equation avoids matrix inversions and speeds convergence by normalizing the variance in all directions [29]. Thus, W is first initialized to the identity matrix I and iteratively updated using the above equation until the change of the matrix is less than a certain threshold.

Generally, when compared on simple simulated data mixing truly independent source signals, they give similar results. When applied to actual data, however, they may produce somewhat different solutions whose significance is hard to evaluate. Several reviews [26][16] have compared various ICA algorithms and their interrelationships. Here, we employ the gradient ascent algorithm as implemented by Makeig *et al.* [29] based on the Infomax algorithm, which has been found to be

effective for analysis of biomedical signals. Algorithm details can be found in [29] and [23].

To evaluate the resulting independent components, back-projection is used to plot body-surface projection maps for each component. From the ICA algorithm, we obtain the unmixing matrix, W. The signal mixing matrix will be W^{-1}, i.e. $x = W^{-1}u$. Let $W^{-1}(:, i)$ denote the i^{th} column of W^{-1}, and $u(i, :)$ denote the i^{th} row of u, then back projection of component i, p_i is:

$$p_i = W^{-1}(:, i) \times u(i, :) \tag{2.5}$$

The column vector $W^{-1}(:, i)$ represents the relative (signed) weight of the i^{th} component in each body-surface channel. The back-projection map of each component may be plotted for each subject.

The computation of back-projection maps is strongly reminiscent of more general body-surface potential mapping (BSPM) techniques, as is the use of high-density electrodes [39]. In BSPM, 32 to 256 ECG electrodes are used to record the body-surface potential field created by the beating heart. The BSPM system has been used in several hundreds of patient recordings representing most common cardiac diseases such as ischemic heart disease, and ventricular and supraventricular arrhythmias [14][15][38]. The main advantage of BSPM, compared to 12-lead ECG, is the ability to visualize the cardiac potential distribution across the whole thorax. Several methods have been proposed for detecting the vulnerability to life-threatening arrhythmias from BSPM recordings and from near-equivalent magnetocardiographic signals [14][15]. In such methods, the signals from each channel are analyzed by signal processing methods such as beat-locked averaging, late potential analysis, spectral turbulence analysis, QRST integral analysis, and spatial parameter mapping.

High-density ECG recording makes more signals available for analysis, necessitating automated signal processing methods and making the method more robust to individual channel noise or dropouts. However, different from previous methods, we visualize the back-projection of each individual ECG source to the body surface, obtained by ICA decomposition, instead of visualizing the sum of these sources, i.e. the whole recorded body-surface signals. The back-projected

component maps may reflect properties of each ECG signal component, providing us with more information about different heart activities compared to BSPM visualizations of the whole signal mixtures.

2.2.2 Back-Projection and Dipole Estimation

To further analyze the components, we use the back projection technique to plot the location maps for each component. From the ICA algorithm, we obtain the unmixing matrix, W, then the mixing matrix will be W^{-1}. Thus, we have $x = W^{-1}u$. Let $W^{-1}(:, i)$ denote the i^{th} column of W^{-1}, and $u(i, :)$ denote the i^{th} row of u, then back projection for component i, p_i can be computed as:

$$p_i = W^{-1}(:, i) \times u(i, :) \tag{2.6}$$

The column vector $W^{-1}(:, i)$ represents the weight of each channel that contributes to the i^{th} decomposed component. We can plot the back projection maps of each component, for each subject.

We also estimate the location and the direction of each source electrical dipole. This will help us follow each source activity according to its corresponding dipole vector. The electrical dipole has separated charges of equal and opposite sign. The vector of electrical dipole is defined as $\vec{P} = q \cdot \vec{d}$, where $\vec{P}$ is the dipole vector; q is the electrical charge of each pole and $\vec{d}$ is the distance vector. Each dipole can be an electrical potential source. The following equation shows how we calculate the potential of a dipole with center O at (x_0, y_0, z_0) from a point A at (x_1, y_1, z_1). Here r is the distance between the dipole center O and point A, as shown in Figure 2.2.

$$f_1(x_1, y_1, z_1) = \frac{1}{4\pi\epsilon_0} \cdot \frac{\vec{P} \cdot \vec{r}}{r^3} = \frac{1}{4\pi\epsilon_0} \cdot \frac{P_x(x_1 - x_0) + P_y(y_1 - y_0) + P_z(z_1 - z_0)}{[(x_1 - x_0)^2 + (y_1 - y_0)^2 + (z_1 - z_0)^2]^{3/2}} \tag{2.7}$$

In our experiments, we have the back projected potential of the i^{th} source as $W_i^{-1} = W^{-1}(:, i)$. Our approach to find the source dipole is as follows.

We model the subject body with an ellipse cylinder as shown in Figure 2.1. Our typical subject cylinder model that matches the ECG electrodes has the height, widths and length of 8, 10 and 6 inches respectively.

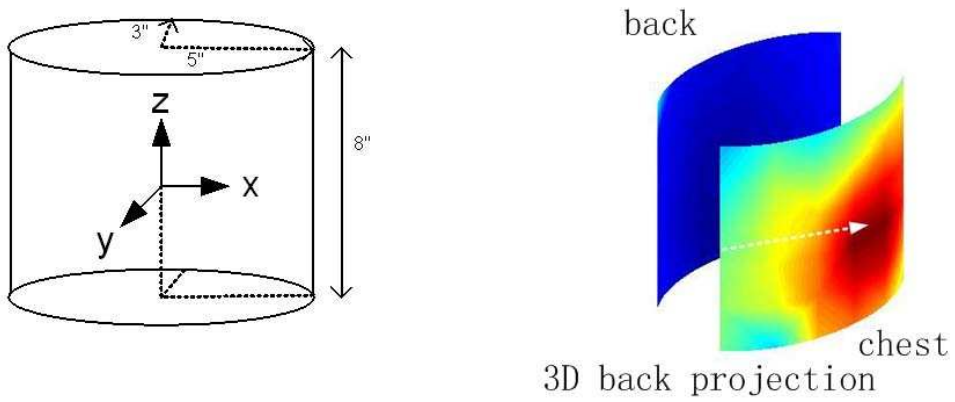

Figure 2.1: Subject Body Ellipse Cylinder Model

We first make an initial guess of the source dipole vector. The source estimation will have the following potential in all the measured points according to equation (2.7):

$$W_i^{-1} = f_i(x_i, y_i, z_i) = \bar{v_i} \tag{2.8}$$

where $\bar{v_i}$ is the estimated potential at point i with the initial value of the dipole vector. The measured value of the potential is W_i^{-1} which we get from the back projection. The difference of the actual and estimated value is defined as $\delta_i = W_i^{-1} - \bar{v_i}$. In our experiments, we have n δ_i for n channels and the objective is to minimize the total difference between the actual and estimated values, normalized by the norm of the vector:

$$F = \frac{\sum_{i=1}^{n} \delta_i^2}{||W_i^{-1}||} \tag{2.9}$$

A simulated annealing algorithm is used to minimize F. The iterative process starts with a random initial solution which consists of the dipole location (x_0, y_0, z_0) and dipole vector direction (P_x, P_y, P_z); in each iteration, neighborhood search is performed with a small perturbation and current temperature decides whether the neighborhood solution is accepted. The decreasing temperature makes the search process more diverse in the beginning and focus on a local area later on. The process is running iteratively until the solution converges.

The pseudo code is shown below. The results are presented in the next section.

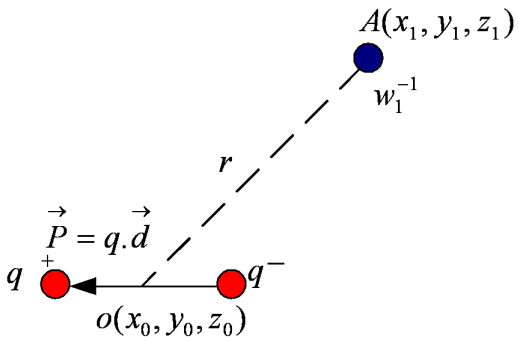

Figure 2.2: Electrical Dipole Vector Potential

```
s := s_0; e := error(s)
                        // initial solution and objective value
t := t_0
                        // initial temperature.
while t > t_terminate
                        // while temperature is not small enough
  s_n := neighbour(s)
                        // neighborhood search
  e_n := error(sn)
                        // neighborhood solution's objective
  if random() < exp((e-e_n)/t) then
                        // should we move to it?
    s := s_n; e := e_n
                        // update solution.
  t = t*0.999
                        // one more evaluation done
return s
```

2.3 Experiments

2.3.1 Equipments & Setup

Our experiments are based on BioSemi's ActiveTwo Base system 2.3 (*http://www.biosemi.com/*). A list of the main necessary equipments is as follows:

- 16×8-*channel amplifier/converter modules*
- 4×32 *pin-type electrodes*
- *Packer Signa electrode gel*
- *128 electrode holders*
- *CMS/DRL electrodes*
- *LabView software*
- *adhesive pads*

The system consists of 128 pin-type electrodes that are designed for use with BioSemi's headcap using the electrode holders (At most 101 of them are used in our experiments). The electrode holders are attached to the skin of the chest and back of the subject by adhesive pads, each by each. The Ag/AgCl electrodes do not require skin preparation, but does require electrode gel to act as a conductor between the skin and the electrodes themselves. The signals recorded by the electrodes are converted and saved in a computer via the AD-box. During the experiments, we set the sampling rate to be 256 points per second.

2.3.2 Procedures

The preliminary experiments are performed on five subjects. We start the experiment with attaching the electrode holders to the chest and back of the subject, forming two identical size matrices. Then adequate amount of electrode gel is injected to the holders before plugging the electrode into them. Three electrodes are placed on the subject's left arm, right arm and left leg as the unipolar limb

Figure 2.3: High Density ECG Recorder

leads to form the Wilson Central Terminal and grounding nodes are placed on the subject's waist, before we connect the electrodes to the AD-box.

When the subject is ready for measurement taking, he is in a relaxed standing position. Although a supine position is ideal in ECG recording, it is not desirable in this case because there is a substantial risk to damage the electrodes that are placed on the back of the subject. The subject is asked to do the following four kinds of activities:

1. Standing still and breathing normally for 90 seconds. It is used as a baseline for comparison to the rest of the activities.

2. Breathing and holding the breath for intervals of 10 seconds alternatively for a period of 90 seconds starting with the breathing interval. It is used to tire out the cardiac muscles so that the contractions of the various muscles will start to separate as shown in the wave forms.

3. Horse stance for a certain period for 60 seconds and record the waveforms after that. Its function is similar to the above but in a more extreme measure.

4. Leaning to different orientations. The first subject is asked to lean forward and left and the rest four subjects are asked to lean in four orientations (forward, backward, left and right). In each orientation 90-second waveforms will be recorded.

In the analysis, we only take the last 50 seconds recording of each activity, because the early phase of activities may contain more noise. We use multiple activities in order to make the heart show different results under different conditions. ICA can then pick up the subtle differences and decompose the waveforms into true source components.

2.4 Experimental Results & Analysis

We performed two experiments on subject 1 to verify the stability of our results.

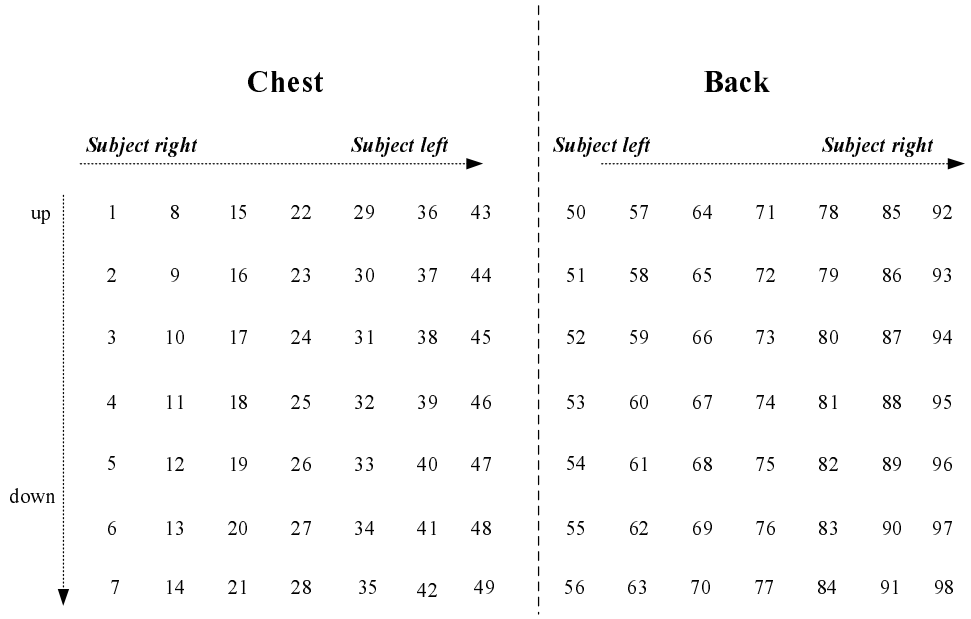

Figure 2.4: Electrode Array Layout on the Subject

We setup the high density electrode probes on the subject chest and back in a 7×7 setup. 98 electrodes (also called channels) are numbered as shown in Figure 2.4 — note that the left and right orientation in the chest and back are reverse since they can form a circle around the body; in the 6×6 case they are arranged in the similar fashion. Figure 2.5 are the photos taken from one of the subjects. For the first subject, we recorded 5 activities: still standing, holding breath, horse stance, leaning forward and left; for the rest four subjects, we recorded 7 activities, with the additional leaning backward and right activities.

The recorded raw data is first processed by two-way least-square FIR (Finite Impulse Response) filtering, with the low-edge frequency in pass band 0.1 Hz and the high-edge frequency in pass band 40 Hz.Figure 2.6 shows the partial recorded raw mixture signals for subject 1. The left portions of the two figures show the wave forms of the still standing phase, and the right portions show the wave forms after horse stance. It is observed that the electrodes on the chest receive much stronger signals than the ones on the back. This is reasonable since

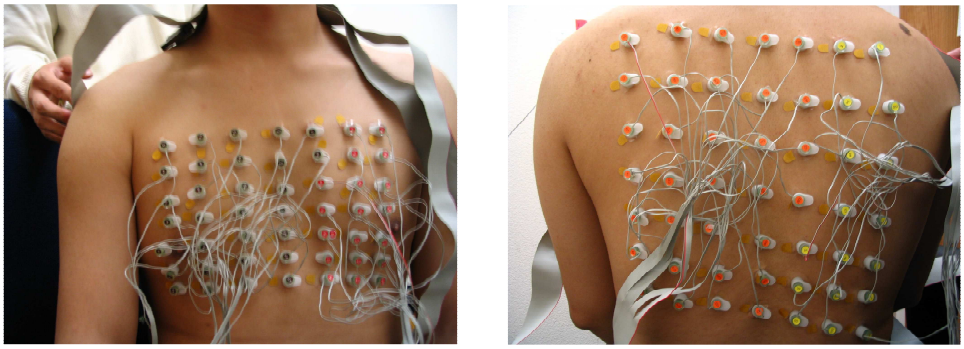

(a) Chest Side (b) Back Side

Figure 2.5: High Density Electrode Setup on the Subject Chest and Back

the human heart is closer to the front of the body.

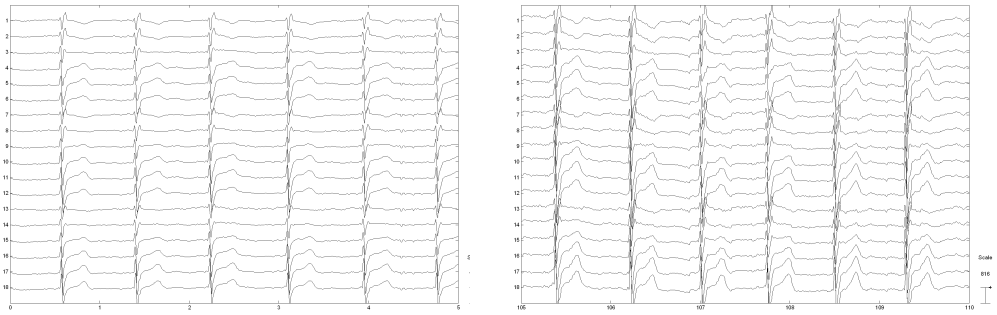

(a) Still Standing (b) Horse Stance

Figure 2.6: Subject 1 Mixture Waveforms

2.4.1 Separated Components

The ICA algorithm is applied to the above two waveforms. By the definition, W is a square matrix (Figure 2.5 and 2.4 , therefore there are 72 and 98 components are produced respectively. However, only a few of them has relatively large amplitude and have meaningful waveforms. We believe the rest of them are generated by breath and noise thus filter them out.

Figure 2.8 shows the meaningful components produced by the ICA algorithm for subject 1. In each figure, the left part shows the 5-second interval and

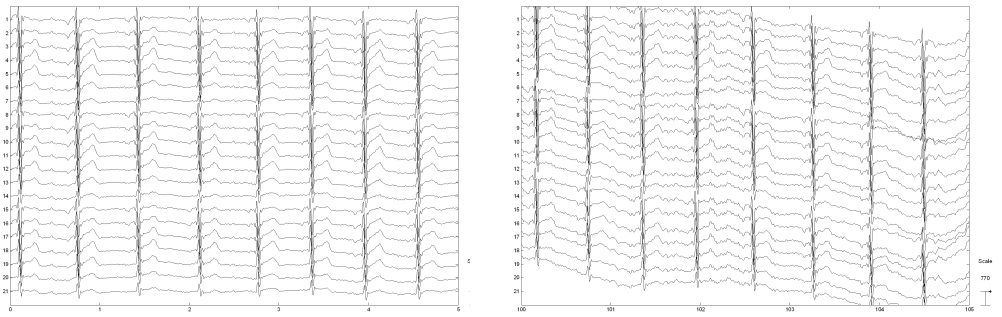

(a) Still Standing (b) Horse Stance

Figure 2.7: Subject 2 Mixture Waveforms

right part shows the 1-second interval to clearly reflect the relationships among different components.

From the results, we have the following observations:

- The ICA algorithm is able to separate P-wave, QRS complex and T-wave. In two experiments, T-wave can be clearly separated. Also, P-wave is successfully separated in the second subject.

- Multiple activities are essential to perform ICA successfully. We have tried different combinations of the waveforms by each activities. The experimental results show that at least three activities are needed to decompose the T-waves and more activities guarantee better separation. This is because different sources would have different behaviors under various circumstances; for example, the shape of the T-waves and its distance from the QRS complex are different in different activities, as shown in Figure 2.6 and Figure 2.7 for the first two subjects.

- The ICA algorithm can detect around 7-8 different components from the original waveforms. Especially, there are multiple components which belong to the QRS components. This phenomenon indicates that the QRS complex wave may be generated by various underlying sources. For subject 2, even the T-wave is decomposed to two components, which shows that even T-wave is probably not a simple activity.

Comp.	1	2	3	4	5	6	7
Exp. 1	0 ms	11.2 ms	23.2 ms	39.0 ms	45.5 ms	59.4 ms	252.4 ms
Exp. 2	0 ms	15.8 ms	28.8 ms	41.3 ms	45.7 ms	63.1 ms	257.9 ms

Table 2.1: Peak Time Difference for the Repeated Experiments on Subject 1

- Note that the components that form the QRS complex have different peak time (they have been sorted in the ascending order of peak time). They could represent a sequence of wave propagation. Thus, it is useful to further analyze these components and detect the physical positions of the sources that produce these components.

In order to show that our experimental results could be stably reproduced, we conducted the same experiments on subject 1 once more. The same analysis was performed on the obtained data. The separated sources are shown in Figure 2.13. We find that we could obtain very similar components from the two experiments in the same subject. Also, we calculate the peak time difference of the components in both experiments, with respect to the peak time of the first component. The results are shown in Table 2.4.1.

It can be observed that the peak time difference among components in the two experiments, which reflects the propagation speed of the heart waves, are very close, except for the 2nd and 3rd components. This shows that our experiments and analysis could be reproduced. The discrepancy on the 2nd and 4th components may be due to the different body conditions or numerical errors, which need to be further investigated.

2.4.2 Back Projection & Dipole Estimation Results

We follow the approach discussed in Section 3 to derive the back-projection body surface potential maps (BSPM) according to the weight of each channel. We also calculated the dipole vector for each component for all the subjects, following the method proposed in Section 3. The dipole location (x_0, y_0, z_0) and the direction (P_x, P_y, P_z) are shown in Table 2. The normalized errors as shown in Equation

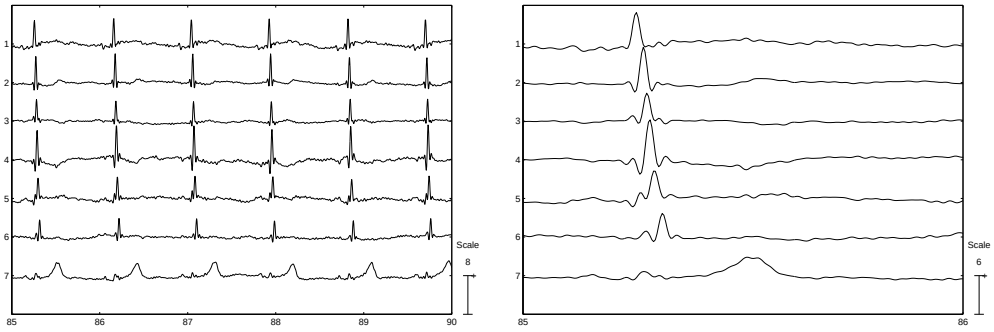

(a) 5-Second Interval (b) 1-Second Interval

Figure 2.8: Source Components for Subject 1

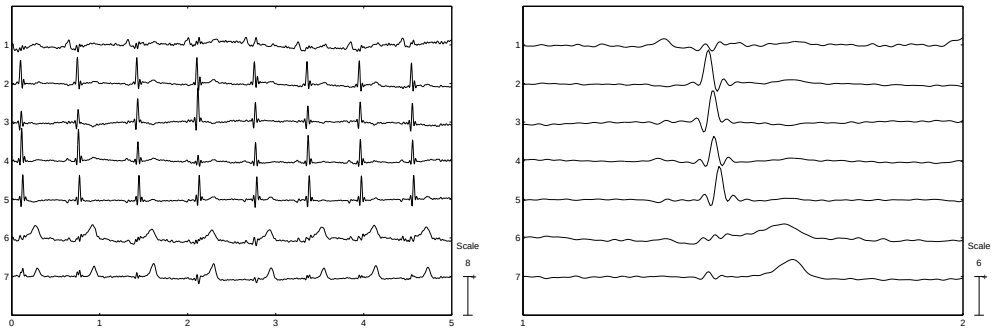

(a) 5-Second Interval (b) 1-Second Interval

Figure 2.9: Source Components for Subject 2

(2.9), are also presented. The last column is the peak time difference of each component, with respect to the first QRS component (therefore the value for P-wave component is negative).

As an example, we plot the back-projection maps, both from the channel weights and dipole estimation, for each component of subject 2. They are shown in Figure 2.14 and 2.15. For each component, the upper left 2D figure is the map plotted according to the channel weights; the lower left 2D figure is the map plotted according to the dipole estimation results. The blue colors denote lower weights and the red color denotes the higher values. When comparing these two figures, we found that they are very similar, which indicates that our estimation is quite accurate. However, the estimated results show the potential distributions are more

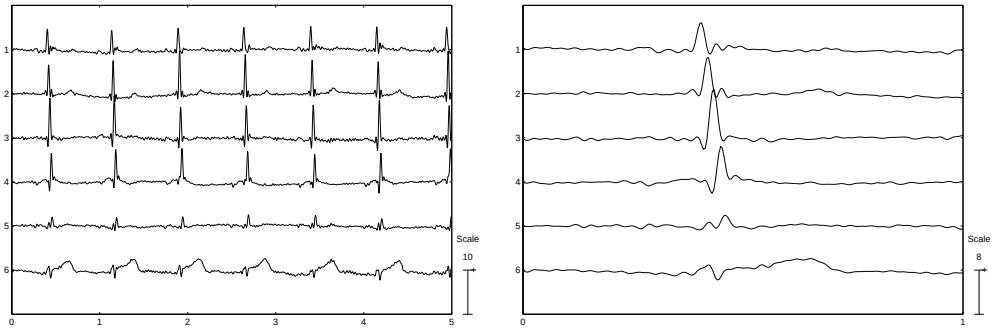

(a) 5-Second Interval (b) 1-Second Interval

Figure 2.10: Source Components for Subject 3

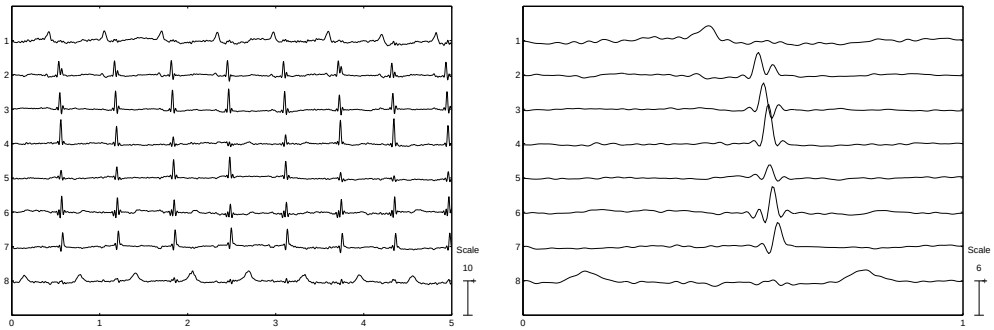

(a) 5-Second Interval (b) 1-Second Interval

Figure 2.11: Source Components for Subject 4

concentrated, which is the nature of the dipole model. This should be the main source of the errors and motivates us to seek for better models.

The differing weights, proportional to different potential values in the body surface, are mapped to different colors, where red represents the largest magnitude and blue represent the smallest one. When plotting, we use finer grid rather than the original two 7×7 matrices and interpolate the values in order to obtain smooth maps.

We also show the 3D (Figure 2.16 and 2.17) maps together with the dipole vectors for all the components. The left 3D map in Figure 2.14 is from the front view and the right one is from the side view. The red dot is the origin of the dipole (x_0, y_0, z_0) and the red vector indicates the direction and relative magnitude

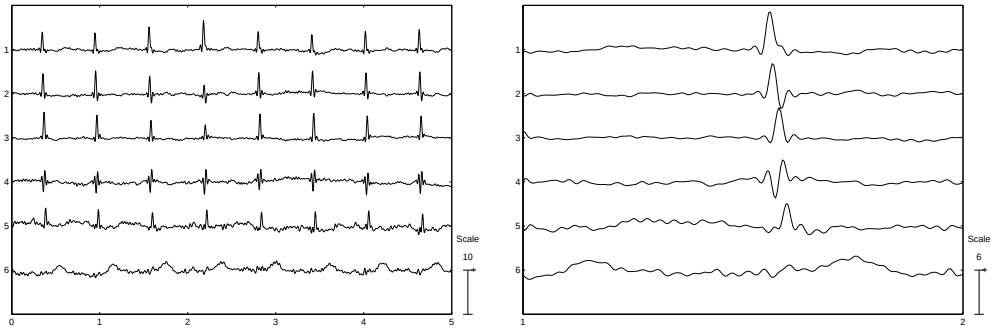

(a) 5-Second Interval (b) 1-Second Interval

Figure 2.12: Source Components for Subject 5

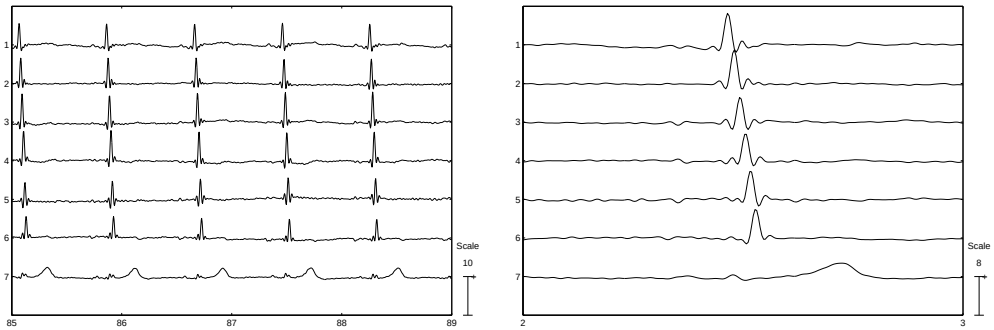

(a) 5-Second Interval (b) 1-Second Interval

Figure 2.13: Source Components for Subject 1 in the Repeated Experiment

of the dipole vector. The green dots show the intersections of the dipole vector and the cylinder bounds. The most right column is the corresponding separated component waveform in the time horizon.

We observe that in most of the maps, the weights are concentrated in the right part of the front chest. This is understandable since it is the closest to the human heart. Furthermore, the most concentrated part, which is highly possible to be the source places that produce these components, is different for different components. The positions of different QRS components are moving downward with the peak waves moving in the time course. And the T-wave sources are located in the lower portion of the maps. This is consistent with the definitions of these waves: QRS complex represents the depolization of the ventricle, and T-wave

indicates the repolization of the ventricle. Since the depolization needs to spread from the AV node to all parts of the ventricles, the sources are moving downward as reflected in the maps of different components of the QRS complex.

The back-projections of different components are computed according to Equation (2.6) and compared with the original channel waveforms. The purpose is to show that the separated components account for different sections of the cardiac cycle. In Fig. 2.18, four different QRS components in Subject 1 are back-projected and over-plotted on the original waveform of one channel. The solid waveforms show the original recorded channel signal, and the dotted waveforms the back-projected component activities. We find that each component accounts for different parts of QRS complex, confirming that ICA separates sources of different sections of the cardiac cycle.

2.5 Discussion & Conclusions

In this work, we design a novel experimental approach to collect stable high-density ECG signals and applied ICA to separate spatially fixed and temporally independent source activities. The results on five subjects show that ICA is able to identify P-wave, T-wave and different parts of QRS complex, and the back-projection and dipole estimation algorithm provides us potential maps of different components which could be used in further analysis.

Although results of applying ICA to high-density ECG have shown great promise, the analysis method still in its infancy. Fruitful directions for further research include:

1. First, we would like to find out what is the best placements for the electrodes to obtain more informative signals. A possibility is to place more electrodes close to the heart and less in the further places. However, non-uniform placement should be based on more knowledge and understanding of the internal mechanism of the human heart.

2. The relationship between the number of electrodes and the performance of source separation and localization should be studied systematically. We have

Subject	**C****	(x_0, y_0, z_0)	(P_x, P_y, P_z)	**Error**	**PTD***
1	1	(1.33, 0.87, -0.62)	(-0.48, 1.26, 0.83)	0.163	0
1	2	(2.86, 0.25, 0.12)	(2.71, 0.84, -1.55)	0.155	11.2
1	3	(0.84, 1.07, 0.15)	(-1.44, -0.96, 0.20)	0.057	23.2
1	4	(0.75, 0.86, -0.19)	(-1.81, -0.77, 0.86)	0.091	39.0
1	5	(0.61, 0.71, -0.25)	(-1.55, -0.55, 1.51)	0.277	45.5
1	6	(3.82, 3.00, 5.00)	(-6.79, -8.14, 4.94)	0.221	59.4
1	7	(1.15, 0.50, 0.32)	(1.95, 0.91, -1.09)	0.132	252.4
2	1	(-0.50, 0.38, 0.60)	(-0.71, 0.10, -2.88)	0.214	-99.2
2	2	(0.62, 0.58, 2.35)	(0.82, 1.23, -1.53)	0.181	0
2	3	(-0.05, 0.63, 4.01)	(0.46, -0.31, 3.06)	0.154	9.3
2	4	(0.28, 0.56, -2.17)	(0.51, -0.53, -2.80)	0.178	12.1
2	5	(0.25, 0.70, -2.36)	(-0.04, -1.06, -2.09)	0.136	25.1
2	6	(0.33, 0.89, 0.61)	(1.31, 0.96, -1.24)	0.097	168.0
2	7	(0.13, 1.16, 0.81)	(1.12, 1.05, -0.42)	0.106	193.9
3	1	(0.87, 0.74, 3.36)	(-0.08, 1.01, -1.92)	0.238	0
3	2	(0.72, 0.62, 5.01)	(3.59, 1.04, 2.44)	0.292	16.7
3	3	(3.05, -2.31, 3.82)	(2.17, -6.11, 0.59)	0.130	30.6
3	4	(0.43, 0.86, -1.08)	(-0.34, -1.30, -1.02)	0.123	46.4
3	5	(0.52, 0.78, 0.67)	(-0.60, -1.45, 0.18)	0.084	56.6
3	6	(0.79, 0.47, 0.73)	(1.68, 1.21, -0.46)	0.124	248.6
4	1	(-0.54, 3.00, 5.50)	(-1.05, 8.15, 1.14)	0.072	-111.3
4	2	(4.32, 2.70, 6.56)	(-9.65, -2.69, 0.36)	0.167	0
4	3	(4.21, 1.56, 5.59)	(9.09, 3.41, -2.56)	0.261	13.0
4	4	(3.19, 0.64, 0.73)	(3.09, 0.37, -1.35)	0.171	26.0
4	5	(3.59, 1.25, 1.95)	(3.35, 1.36, -0.79)	0.310	29.7
4	6	(1.01, 1.31, -0.43)	(1.20, -0.51, -1.06)	0.183	34.3
4	7	(-0.27, 0.22, 0.12)	(0.14, -1.26, 0.96)	0.406	45.5
4	8	(0.82, 1.47, 1.77)	(0.70, 0.61, -1.09)	0.192	242.1
5	1	(-0.73, 0.87, 2.12)	(0.58, -0.31, 2.67)	0.117	0
5	2	(-0.42, 0.72, 2.11)	(0.50, -0.26, 2.96)	0.120	9.28
5	3	(-0.28, 0.92, 1.36)	(0.23, -0.92, 1.98)	0.088	20.4
5	4	(0.28, -0.18, 0.40)	(-0.47, -1.56, -0.30)	0.184	29.7
5	5	(-0.55, 0.78, 2.40)	(-0.00, -1.15, 1.68)	0.145	40.8
5	6	(-0.62, 0.86, 0.37)	(0.14, 1.39, 1.00)	0.049	199.5

Table 2.2: Estimated Dipole and Peak Time Difference for Each Component; PTD*: Peak Time Difference, in the unit of micro second ; C** : Component

Subject	**C****	$d(x_0, y_0, z_0)/dt$	$d(P_x, P_y, P_z)/dt$
1	1	-	-
1	2	(0.137, -0.055, 0.066)	(0.199, -0.038, -0.213)
1	3	(-0.168, 0.068, 0.003)	(-0.106, -0.150, 0.146)
1	4	(-0.006, -0.013, -0.022)	(-0.206, 0.012, 0.042)
1	5	(-0.022, -0.023, -0.009)	(0.040, 0.034, 0.100)
1	6	(0.231, 0.165, 0.378)	(-0.377, -0.546, 0.247)
1	7	(-0.014, -0.013, -0.024)	(0.045, 0.047, -0.031)
2	1	-	-
2	2	(0.011, 0.002, 0.018)	(0.015, 0.011, 0.014)
2	3	(-0.072, 0.005, 0.178)	(-0.039, -0.166, 0.494)
2	4	(0.218, -0.025, -2.207)	(0.018, -0.079, -2.093)
2	5	(-0.024, 0.011, -0.015)	(-0.042, -0.041, 0.055)
2	6	(0.001, 0.001, 0.021)	(0.009, 0.014, 0.006)
2	7	(-0.008, 0.010, 0.008)	(-0.007, 0.003, 0.032)
3	1	-	-
3	2	(-0.009, -0.007, 0.099)	(0.220, 0.002, 0.261)
3	3	(0.168, -0.211, -0.086)	(-0.102, -0.514, -0.133)
3	4	(-0.166, 0.201, -0.310)	(-0.159, 0.304, -0.102)
3	5	(0.009, -0.008, 0.172)	(-0.025, -0.015, 0.118)
3	6	(0.001, -0.002, 0.000)	(0.012, 0.014, -0.003)
4	1	-	-
4	2	(0.044, -0.003, 0.010)	(0.004, -0.097, -0.007)
4	3	(-0.008, -0.088, -0.075)	(0.749, 0.469, -0.232)
4	4	(-0.078, -0.071, -0.374)	(-0.462, -0.234, 0.100)
4	5	(0.108, 0.165, 0.330)	(0.070, 0.268, 0.151)
4	6	(-0.561, 0.013, -0.517)	(-0.467, -0.407, -0.059)
4	7	(-0.114, -0.097, 0.049)	(-0.095, -0.067, 0.180)
4	8	(0.006, 0.006, 0.008)	(0.003, 0.010, -0.010)
5	1	-	-
5	2	(0.033, -0.016, -0.001)	(-0.009, 0.005, 0.031)
5	3	(0.013, 0.018, -0.067)	(-0.024, -0.059, -0.088)
5	4	(0.060, -0.118, -0.103)	(-0.075, -0.069, -0.245)
5	5	(-0.075, 0.086, 0.180)	(0.042, 0.037, 0.178)
5	6	(-0.000, 0.001, -0.013)	(0.001, 0.016, -0.004)

Table 2.3: Estimated Dipole Derivatives for Each Component ; C** : Component

tried to reduce the number of electrodes but found the results become inferior [37]. But, it was not done systematically. We plan to perform a comprehensive study to assess the performance of ICA as a function of the number of sensors in the follow-on research because in the real clinical applications, we always prefer to reduce the number of channels in order to save the operational efforts as well as cost without sacrificing the accuracy of diagnosis.

3. It is also of importance to discover to what extent different cardiac sources can be decomposed, with the different activities. Currently 7 conditions are used in the experiments and P-wave, T-wave and QRS complex could be separated. It is interesting to know whether these components are "atomic", i.e. whether each of them is generated by a single source of the heart and consequently could not be further decomposed. The possible ways to validate this conjecture include design more activities in the experiments to acquire more data for ICA, or try different algorithms other than ICA to decompose the mixed signals.

4. Enhancing the dipole estimation process will be beneficial in the analysis. The cylinder model is probably a bit coarse to depict the human body. A two-sphere model, which considers both the human body and the heart, could represent the nature of the human more accurately. However, the dipole estimation formula and algorithm should be revised and the computational complexity is inevitably increased, which demands further research.

5. The sources obtained by ICA could be verified using the intercardiac signals. We need to work with electrophysiologists to get simultaneous high-density surface ECG and intercardiac recordings on patients, so that we can verify the source activities obtained by ICA. If our approach could be validated in this rigorous process, it would be better accepted in the practical clinical diagnosis, since it is non-invasive and cost-effective, and the analysis is automated and results are informative and fully visualized.

2.6 Spatial Density Reduction in the Study of the ECG Signals

In our project, we use independent component analysis to study the electrocardiogram (ECG) signal of the human heart. ECG is an important tool in diagnosing heart diseases. Currently, 12-lead ECG is commonly used which can only record limited aspects of the heart electrical signals. Previously, an approach for the analysis of the ECG signal using high spatial resolution using 101 or 75 channels on the chest and back of the subject for recording the heart signal has been proposed by *Zhu* et al [44]. They can decompose the original signal into distinct temporal source components by applying independent component analysis (ICA). Using back projection, They can further analyze the activities of each source component on the subject surface. In this paper, we reduce the number of recording channels to 24 and 12 while still able to decompose the ECG signal into similar source components. This approach facilitates the feasibility of the ICA study on the subject patients with moderate spatial resolution, since it requires significantly fewer leads for recording and easier diagnosis setup. Also, we propose a method to estimate the source components dipoles based on the gradient descent method.

2.6.1 Overview

Having an efficient model that can represent the electrical activities of the human heart has been the topic of the medical research for decades. Having a reasonable model for heart signals will help the medical doctors in their diagnosis and will allow them to determine the problem and maybe the point of failure on the heart wall. The electrocardiograph (ECG) is a method to perform measurements on patients in a noninvasive manner without surgery and is therefore simple, fast and cost effective. Doctors use ECG to determine the amount of electrical signal reaching at each point of the body during each activity. The issue is that sometimes a healthy subject can have an abnormal heart rhythm when a patient with a heart disease has a normal heart rhythm. Therefore, focusing on only

one channel is not sufficient for the representation of the whole heart activity. To have a more efficient analysis you need to decompose the heart signals into the source components and determine the contribution of each component to the heart activity in different body regions. Currently, for the purpose of our study we use independent component analysis (ICA) which is a technique for performing blind source separation of the statistically independent sources [16]. Previously, there has been research on the multi channel recordings to study human heart activity [32], [27], [28] but there were not many that used a high density electrodes to decompose the independent components . *Zhu* et al [44] used two square matrices of channels on the subject chest and back to identify different components of the heart signal using ICA. They were able to decompose the ECG signal into P-wave, QRS complex and T-wave because they recorded high density input channels. They then applied source components corresponding back projection to demonstrate different properties of the source on the subject body as an affective way to locate the underlying problems of the human heart compared to a normal ECG. Having many channels is a limitation in their study, which makes the experiment setup slow and difficult. In this work, we try to minimize the number of the channels which we use in our experiment while still able to decompose the same ICA source signals. We try to identify the location and numbers of the proper leads which are sufficient for running our experiment. It turns out that we can reduce many redundant channel recording and get reasonable same separation. Even though, we are not using traditional 12-lead ECG but we get fairly reasonable results with using slightly more channels which are 12 and 24 in our experiments. By this way we would have a simple and faster heart study experiment which makes it practical for the diagnosis. We also propose a method for calculating the electrical dipoles of the source components using the Nelder-Mead simplex method [30]. In the section II, our experiment setup and results will be discussed, and next, we will talk about the future work and direction in section III.

2.6.2 Experiment

Setup and Procedure

In our experiment, we use BioSemi's ActiveTwo Base electrophysiological recording system. The system includes 128 pin-type electrodes that are designed for BioSemi's headcap using the CMS/DRL electrode holders. In our experiment we use at most 101 of them. The electrodes are connected to the chest and back of the subject using adhesive pads. The electrodes are connected to a 256 AD-box which is powered by battery. The AD-box provides the measurement outputs through a USB2 connection to the connected computer. The data is saved via LabView software for our analysis. We use 256 point per second as our sampling rate.

Original measurements were done on the chest and back of the subject in the form of two 7×7 or 6×6 identical square matrix as in 2. We connect the electrodes to the skin of the subject using adhesive pads. We also, connect three additional loose electrodes on the subject left arm, right arm and left leg as the unipolar limb leads to form the Wilson Central Terminal and place the electrodes CMS/DRL on the subject's waist as the active grounding electrode. The electrodes are then connected to the AD-box for the recording.

emphZhu at al [44] used 98 channels to perform a noninvasive study of the ECG signal. We followed similar experiment setup and used 98 channels in the form of two 7×7 identical square matrices placed on the subject chest and back. We set the sampling rate of the ECG recorder to 256 points per second. Five healthy subjected participated in this study. The subjects performed four major activities during the recording: standing still, holding and releasing breathe, horse stance position and finally leaning to four directions. During the later activities, the cardiac muscles are tired and contracted. We use the last 50 seconds of our recording for each activity analysis since the earlier recordings probably contain the transient movement artifacts. Multiple activities give us a better variation in time domain which helps the convergence of ICA training. In the next section, we present the result from the measurements as a baseline.

Results and Analysis

In our experiment, we originally used 7×7 electrodes on the subject chest and back. We use the following number sequence for the electrodes input matrix which is shown in the Figure 2.19:

The recorded raw data is first processed by two-way least-square FIR (Finite Impulse Response) filtering, with the low-edge frequency in the pass band 0.1 Hz and the high frequency edge is in pass band 40 Hz. When we look at the raw data, we see that the first four columns on the left side of the subject's chest have stronger input signals. The first three columns on the right chest and most of the upper back chest have relatively weaker input signals. In most of the subjects the lower back signals are very week. We consider this in our current experiment. We have previously shown in [44], that ICA can decompose the 98 input signals into source components. ICA separates the P-wave form, QRS-complex and T-wave form successfully. However only a few of the decomposed components have relatively large amplitude and have meaningful data (Figure 2.20). We believe that the rest of the sources are generated by noise and breath and thus we filter them out (Figure 2.21).

In our current experiment, we tried different patterns and combinations of the input signals and applied ICA on them. For our input we emphasize on the regions with relative strong input signals. First, we tried different patterns of the 48 input signals. We observed that the majority of the decomposed signals are still not meaningful. Therefore, we have tried combinations of the 24 channels, 12 channels and 6 channels Next, we tried various combinations of the 24 channel input signals for the ICA. ICA was able to decompose the P-wave, QRS and T-wave. Figures 2.22 , 2.23 , 2.24 and 2.25 show the results from the ICA decomposition.

Here, we obtained more meaningful separation and less noise. We ran some experiments with just focusing on the four strong input front left columns. It turns out that even though the inputs are relatively strong compared to other regions, since there is less signal variation, we do not have a good ICA separation compare to using different regions combination. Also, most of the back signals contribute to QRS-complex; and because of less signal variation using them lonely is not

much helpful in ICA. The heart location is closer to front chest, and therefore back channels should be used in combination with front signals to get a better decomposition result. We have better ICA separation, when we used combination of the upper right chest, with more signals from left chest and a few channels from back left. This matches the original position of the heart on the chest which is from middle right to lower left.

Also, QRS-complex and T-wave are decomposed into more than one source which indicates that they are not simple activities. The peak of the QRS-complex varies which represents a sequence of the wave propagation. Decomposing of the P-wave is very difficult and only in few patterns, we are able to decompose P-wave. P-wave is initiated from SA node and atrial depolarization and thus it is better to choose 1 or 2 channels from the upper middle positions where in Figure 2.19 begins with element 15 and 22 in the 7×7 matrix.

We then reduced the number of channels for the ICA to 12. If we use right input combination we are still able to get a good ECG separation. The proper patterns are those which have 2 to 3 channels from upper right chest, 7 to 9 from left of the subject chest and 1 to 2 from back left (Figures 2.22 , 2.23 , 2.24 and 2.25).

When we use different combination of the 6 channels patterns, we are not able to decompose and separate P-wave, QRS complex and T-wave completely. This confirms our original idea that commonly-used 12-lead ECG is not sufficient for the ICA decomposition.

Back Projection and Dipole

To analyze the back location of each component, we need to do back projection. From ICA we obtain the unmixing matrix W. The mixing matrix will be then W^{-1} and $x = W^{-1} \cdot u$. Here, $W^{-1}(:, i)$ denotes i^{th} column of the W^{-1} and $u(i, :)$ corresponds to the i^{th} row of the source. Then back projection for the component i, p_i is calculated as:

$$p_i = W^{-1}(:, i) \times u(i, :) \tag{2.10}$$

The column vector $W^{-1}(:, i)$ represents the weight of each channel that contributes to the i^{th} decomposed component. Here, since we have only 12 or 24 channels we only plot the corresponding columns of the 12 or 24 channels decomposition result. In the back projection maps, the blue colors denote lower weights and the red color denotes the higher weights. The back projection peak (Figure **??**) follows the same pattern as the source back projection of the components in the 98 channels in section 2. In this section, we estimate the location and the direction of the each source electrical dipole. This will help us follow each source activity according to its corresponding dipole vector. The electrical dipole has separated charges of equal and opposite sign. The vector of electrical dipole is defined as $\overrightarrow{P} = q \cdot \overrightarrow{d}$ where $\overrightarrow{P}$ is the dipole vector; q is the electrical charge of each pole and $\overrightarrow{d}$ is the distance vector. Each dipole can be an electrical potential source. The following shows how we calculate the potential of a dipole with center O at (x_0, y_0, z_0) from a point A in (x_1, y_1, z_1). Here r is the distance of dipole center O from point A (Figure 2.2)

$$f_i(x_i, y_i, y_i) = \frac{1}{4\pi\varepsilon_0}.\frac{\overline{p} \cdot \overline{r}}{r^3} \tag{2.11}$$

In our experiments we have the back projected potential of i^{th} source for 12 channels or 24 channels as W_i^{-1}. Our algorithm to find the source dipole is as following: We model the subject body with an eclipse cylinder according to Figure 2.1. Our typical subject cylinder model that matches the ECG electrodes has the height, width and length of 8, 10 and 6 inches. We first make an initial guess for the source dipole vector. The source estimation will have the following potential in 12 points according to equation 2.11:

$$W^{-1} = f_i(x_i, y_i, y_i) = \overline{v}_i; 1 \leq i \leq 12 \tag{2.12}$$

Here $\overline{v}_i$ is the estimated potential at point i with the initial value of the dipole vector. The measured value of the potential is W_i^{-1} which we get from the back projection. The difference of the actual and estimated value is defined as $\delta_i = W^{-1} - \overline{v_i}$. We have 12 δ_i for 12 reduced point and we try to minimize the difference between actual and estimated value 2.12:

vector	source 1	source 2	source 3	source 4	source 5	source 6
O_x	-1.1426	-0.83987	-0.064677	1.87E-09	0.05914	-0.76622
O_y	-1.3654	-0.64782	0.51696	-1.00E-10	-0.53588	-0.14421
O_z	0.54073	0.18784	0.15424	-3.53E-10	-0.57537	0.94966
P_x	7.29E-09	2.43E-09	6.42E-10	1.90E-09	-2.51E-09	7.95E-09
P_y	-8.69E-10	4.25E-10	-9.38E-10	2.85E-10	2.58E-09	-2.91E-09
P_z	-1.70E-10	-1.70E-10	-4.78E-10	-2.59E-10	-2.59E-10	-3.31E-09

Table 2.4: Dipole vector estimation for the 12 channel

$$\sum_{i=1}^{12} f_i = \delta_1^2 + ... + \delta_1^1 2 \tag{2.13}$$

In order to find the minimum of the 2.13 for all the 12 points we use the simplex method [30] which is an optimization method for minimization. It takes iterative steps proportional to the negative of the function gradient in order to find the local minimum. Using the descent gradient we are able to both find the dipole location (x_0, y_0, z_0) and dipole vector direction (p_x, p_y, p_z) . As an example in pattern 3 of 12 channels, having the reference of the ellipse cylinder in the center of the body and using above dimensions for a typical subject, we have estimated the center of the dipole in Table 2.6.2.

2.6.3 Discussions and conclusions

The successful result from applying ICA to the electroencephalographic (EEG) signals inspired us to use ICA to study the ECG signal of the multiple channels. Setting up the experiments for high spatial resolution is not easy. Here, we show that even though traditional 12 lead ECG channel is not sufficient for the decomposition of the P-wave, QRS-complex and T-wave, using 12 and 24 channels, choosing proper patterns are successful in the ICA separation. The choice of the channels is based on the location and strength of the source mixed signals. We choose few channels from upper right side of the chest, most of our channels from left of the subject chest and few from back left. In this way, using only 12 or 24 channels we can get reasonable ICA decomposition which is comparable to our

original 98 ICA experiments. Setting up the experiments for high spatial resolution is time-consuming and complicated. Our current study show that even though traditional 12-lead ECG is not sufficient for the decomposition of the P-wave, QRS-complex and T-wave, we can obtain a successful ICA separation by choosing 12-24 informative channels placed on the chest and back of the subjects. We have a simple homogenous cylinder body model compare to two spheres models for subject and heart, therefore further assumptions need to take into account to be able to estimate the dipole for 12 channels which we will consider it as a future work. This methodology enables the practical setup of the ICA of ECG in a much easier and faster way. Both dipole and back projections BSPM could be used for the further analysis of the ECG source components and might be beneficial for the diagnosis of cardiac diseases [37].

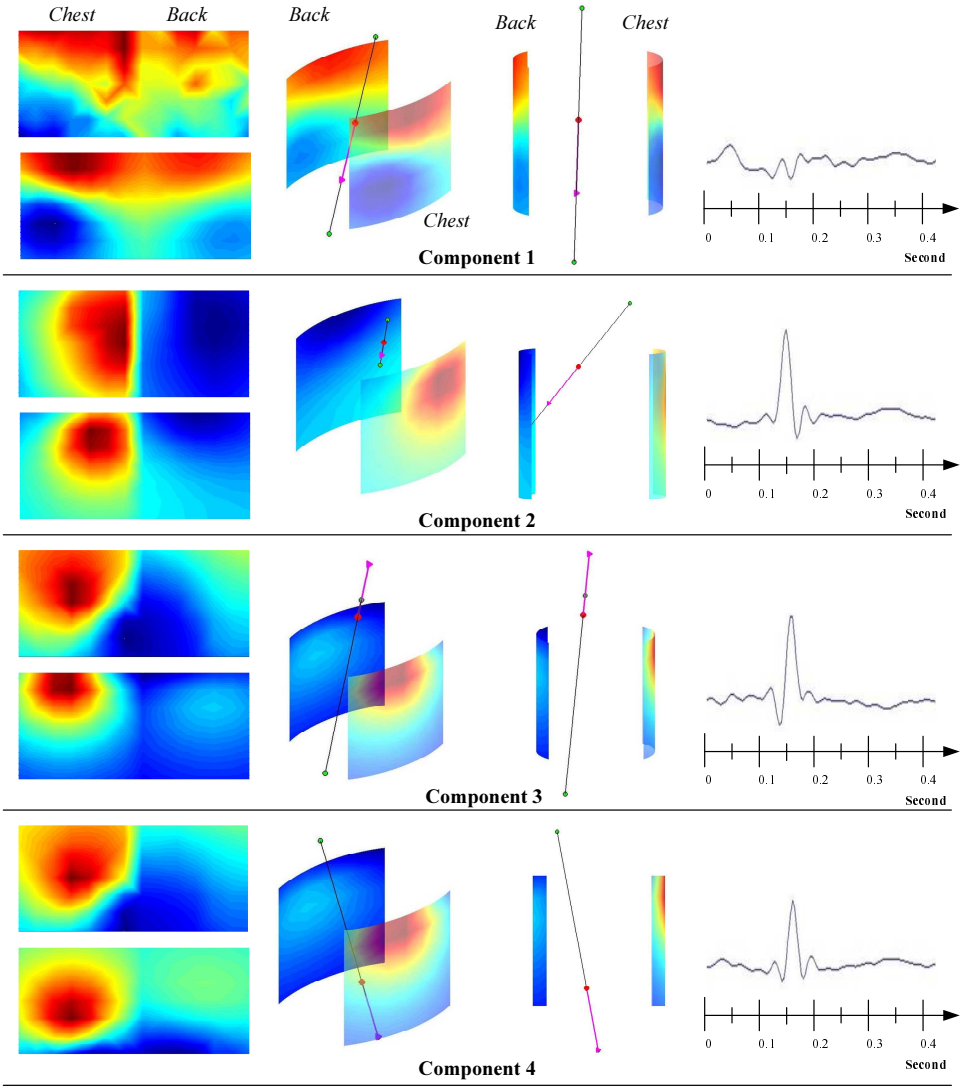

Figure 2.14: Back Projection Maps for Subject 2 (Components 1 – 4)

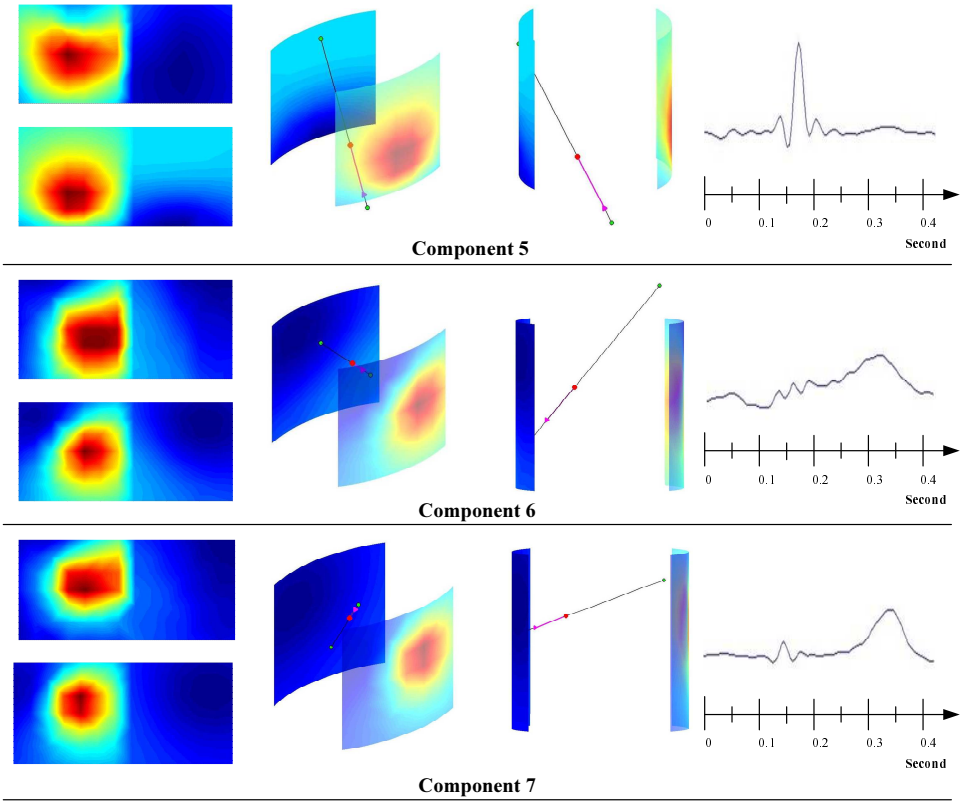

Figure 2.15: Back Projection Maps for Subject 2 (Components 5 – 7)

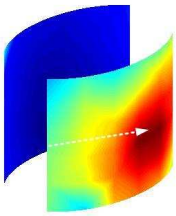

(a) Component 1 3-D Map

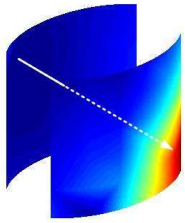

(b) Component 2 3-D Map

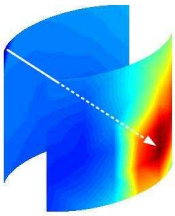

(c) Component 3 3-D Map

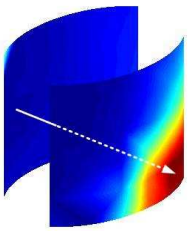

(d) Component 4 3-D Map

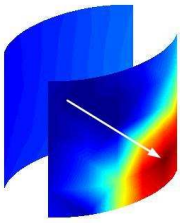

(e) Component 5 3-D Map

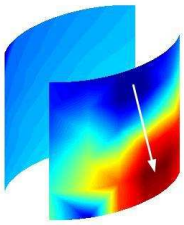

(f) Component 6 3-D Map

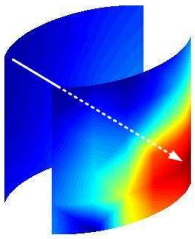

(g) Component 7 3-D Map

Figure 2.16: Subject 1 3-D Back Projection

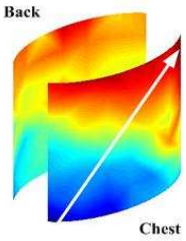

(a) Component 1 3-D Map

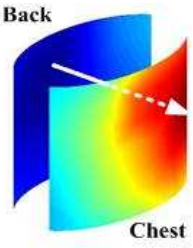

(b) Component 2 3-D Map

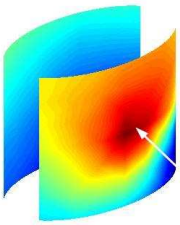

(c) Component 3 3-D Map

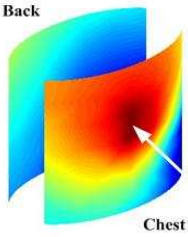

(d) Component 4 3-D Map

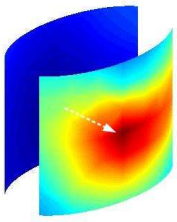

(e) Component 5 3-D Map

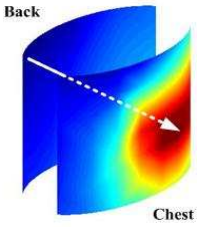

(f) Component 6 3-D Map

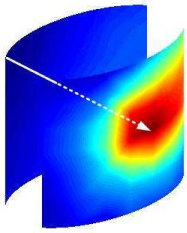

(g) Component 7 3-D Map

Figure 2.17: Subject 2 3-D Back Projection

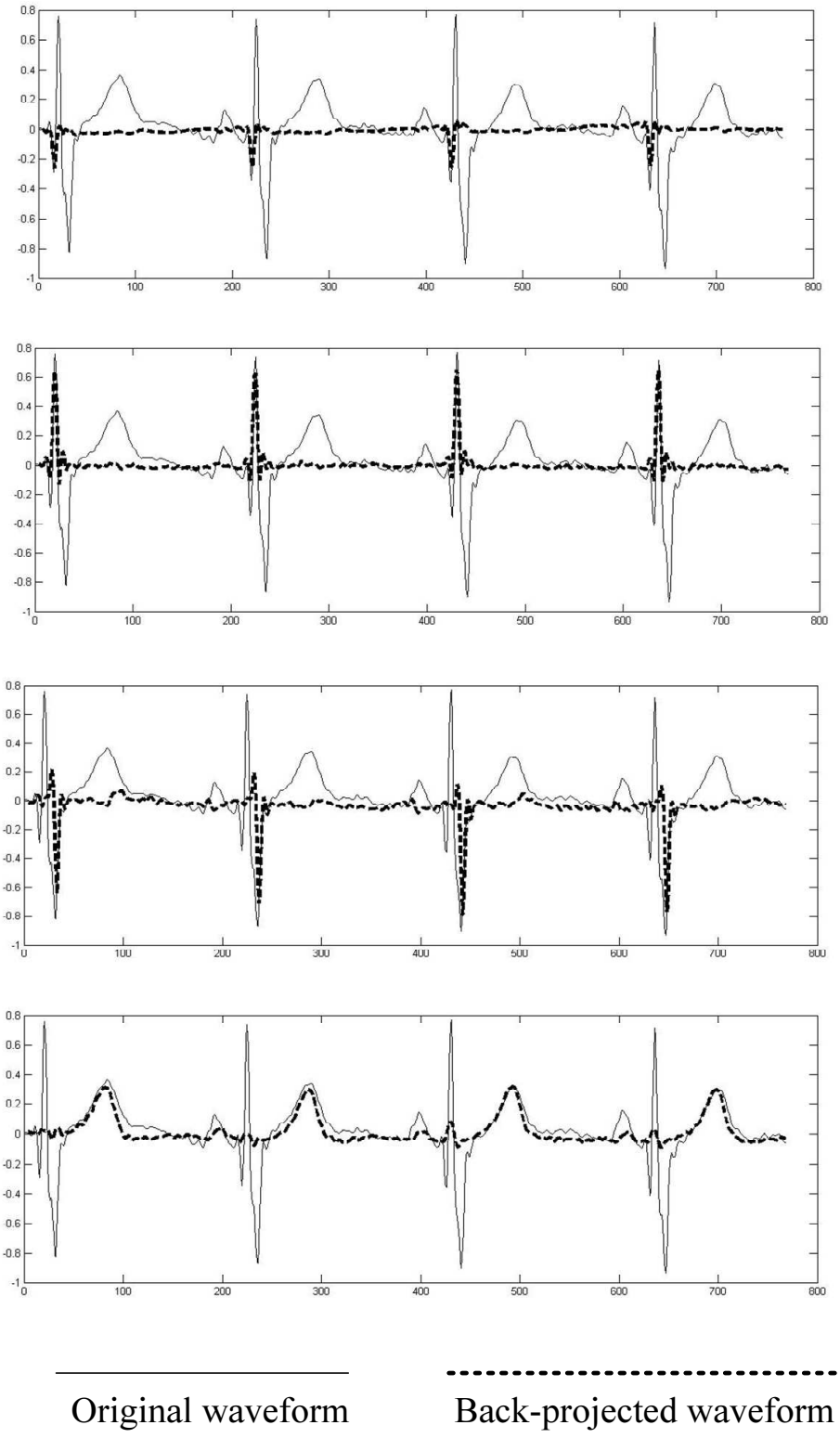

Figure 2.18: Over-plot Back-Projected Components on a Specific Channel

right of chest						left of chest
1	8	15	22	29	36	43
2	9	16	23	30	37	44
3	10	17	24	31	38	45
4	11	18	25	32	39	46
5	12	19	26	33	40	47
6	13	20	27	34	41	48
7	14	21	28	35	42	49

weak source signal
average source signal
strong source signal

left of back						right of back
50	57	64	71	78	85	92
51	58	65	72	79	86	93
52	59	66	73	80	87	94
53	60	67	74	81	88	95
54	61	68	75	82	89	96
55	62	69	76	83	90	97
56	63	70	77	84	91	98

Figure 2.19: Signal Map for the 7x7 Layout

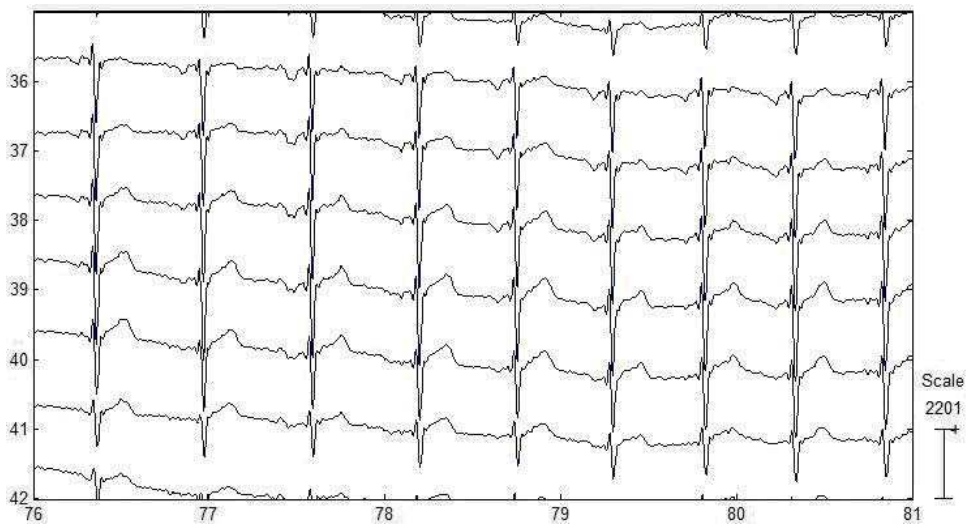

Figure 2.20: Breath and hold strong source signal channels 36 to 42

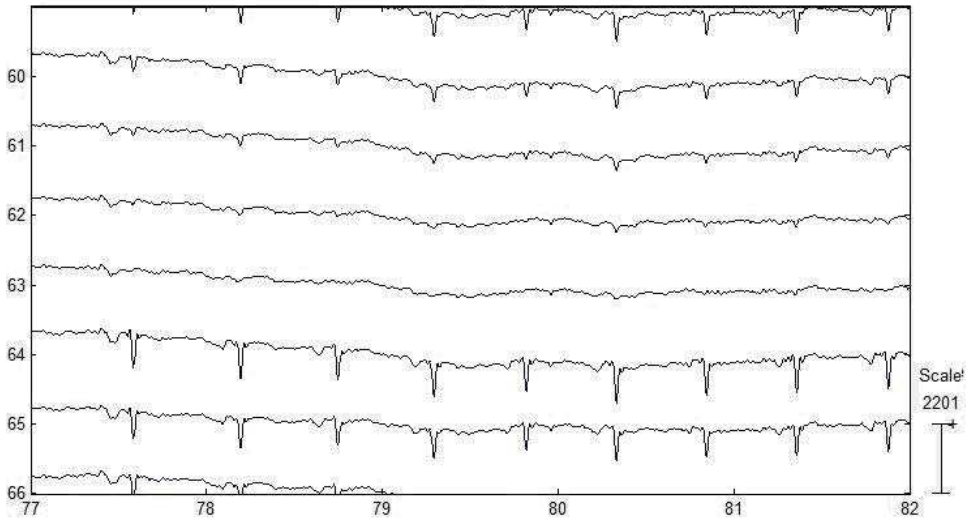

Figure 2.21: Weak source mixture signal channels 60 to 65

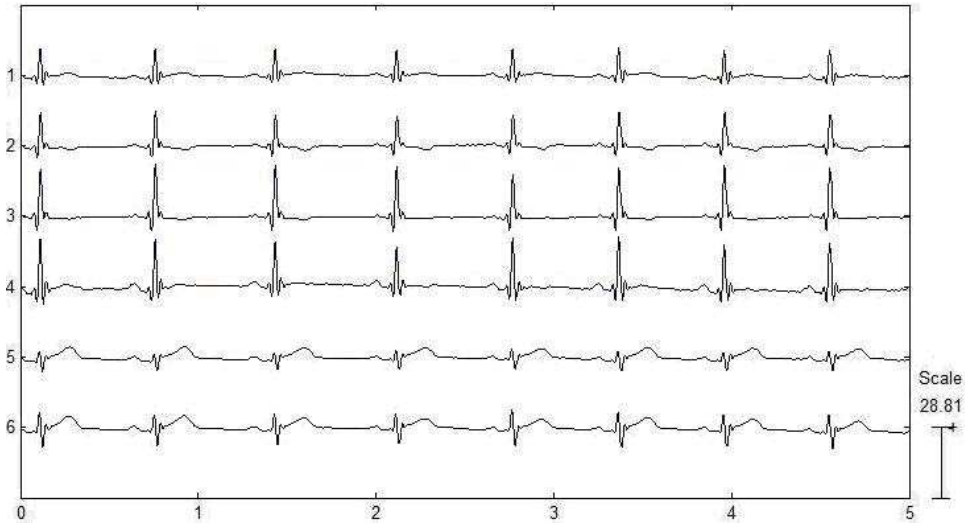

Figure 2.22: Decomposed Pattern 1 source components for 12 channels

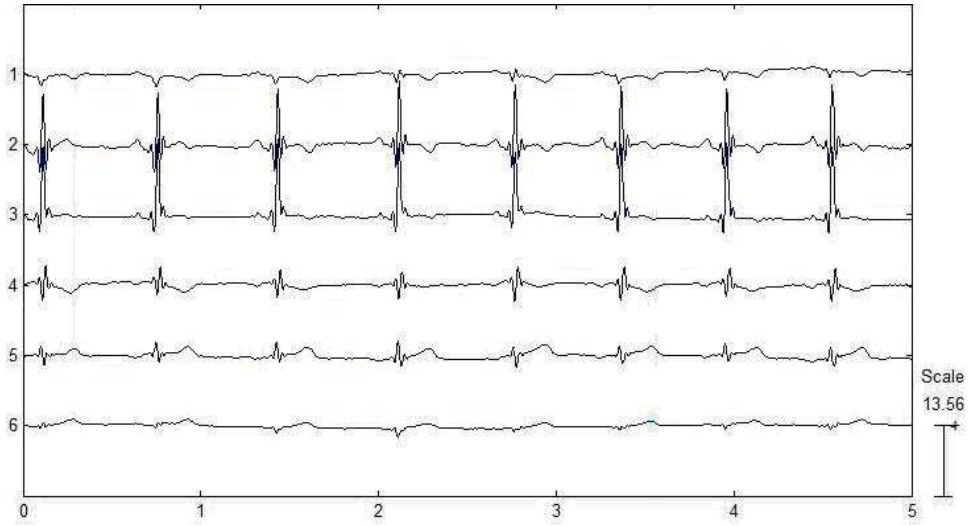

Figure 2.23: Decomposed Pattern 2 source components for 12 channels

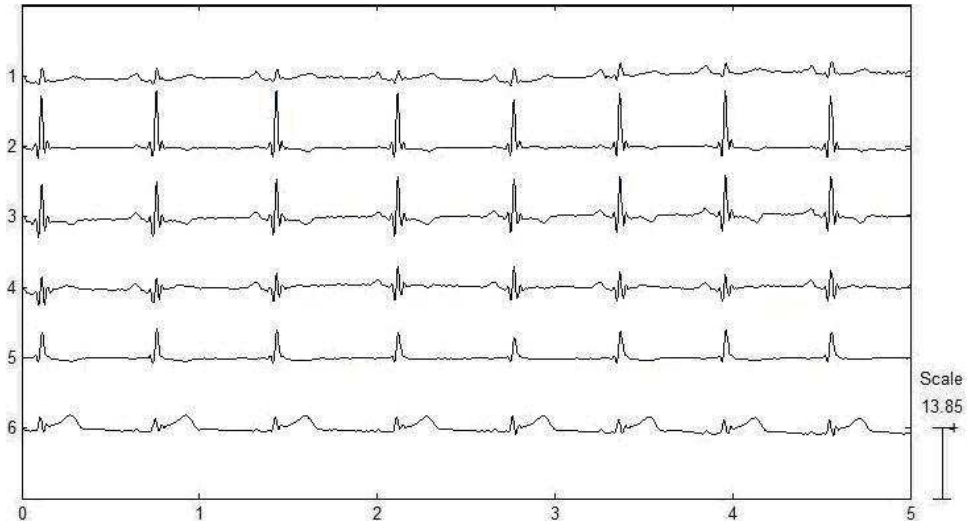

Figure 2.24: Decomposed Pattern 3 source components for 24 channels

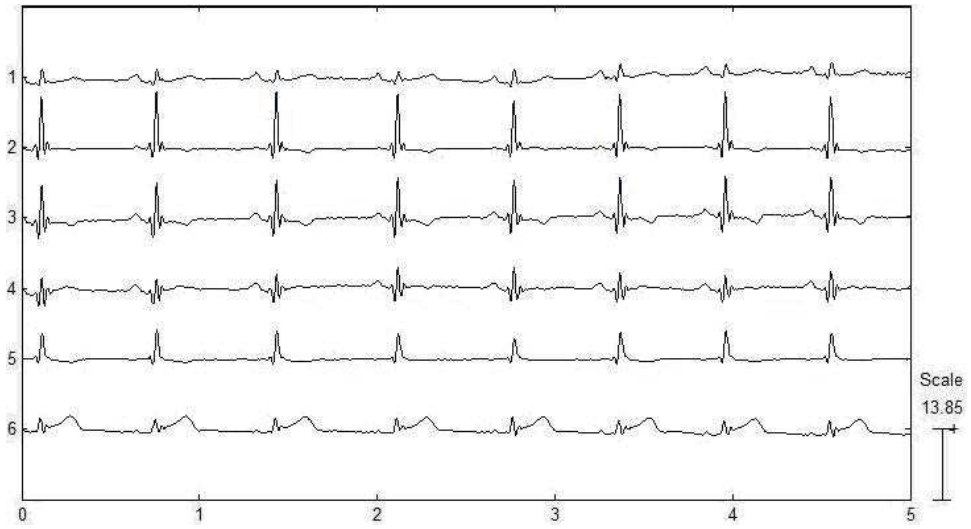

Figure 2.25: Decomposed Pattern 4 source components for 24 channels

3

High Density Cardioneural Signal Experiment

Heart activities are governed by the sympathetic and parasympathetic nervous system. Changes in these neural signals influence the development of arrhythmias, including ventricular tachyarrhythmias that often progress to sudden cardiac death (SDC). A simultaneous study of the cardioneural signals with the electrical heart activity can elucidate the mechanism of abnormal heart activity. In this work, we identify the locations to detect cardioneural signals. We first perform a 108 channel measurement to explore the cardioneural signals. We then focus on selected locations for longer period measurement. We monitor the changes in the heart rate following each sympathetic or vagal nerve activity. The neural signals are extracted from ECG by applying independent component analysis. The work provides a promising approach for studying the association of cardioneural signals with electrical heart activity.

3.1 Cardioneural signal overview

Neurons are electrically excitable cells in the nervous system that process and transmit information. Both sympathetic and parasympathetic nervous systems impact the activity and beat rate of the heart. Damage to nerves extrinsic to the heart, such as the stellate ganglia, as well as to intrinsic cardiac nerves from

diseases that may affect nerves primarily, such as viral infections, or secondarily, from the disease that cause cardiac damage, may produce cardio neuropathy. *Cao* et al 's [4] study show that in most cases, the direct cause of sudden cardiac death (SDC), is ventricular fibrillation which is usually preceded by ventricular tachycardia (VT). Also, the nerve fiber density and regional sympathetic hyperinnervation in the ventricles is correlated with the occurrence of spontaneous ventricular tachyarrythmia or SDC [5]. Such neuron changes may create electrical instability through a variety of electrophysiological mechanisms. For instance, myocardial infraction can interrupt afferent and efferent neural transmission and create areas of sympathetic super sensitivity that may be conductive to the development of the arrhythmias [3].

Being able to measure neuron signal and Electrocardiogram (ECG) signal simultaneously in a non-invasive method will help doctors to easily determine the problem or perhaps point out which part of the neuron systems or heart is failing. Non-invasive measurement is more cost effective for patients and is also much faster and simpler to prepare and perform than invasive measurements that require surgery.

Recording biomedical signals using multiple electrodes will enable us to obtain a spatial description of biomedical phenomenon. Since the activity of the excitable cells is viewed from a distance from the electrodes, with different tissues in between such as blood, skeletal muscles, bone, it is impossible to non-invasively determine detailed information about the cellular properties and propagation patterns. Consequently, significant empirical knowledge is required for crucial clinical decision making. In order to address these issues, we propose an approach to perform non-invasive simultaneous study of neural and ECG signals by applying independent component analysis (ICA).

Neural signals are usually contaminated in the measurement by the Electrocardiogram signals (ECG) of the heart. In our experiments, we record both ECG and neuron signals in a non-invasive manner. The recorded neural signals exhibit the presence of ECG. For improved analysis of the neuron signals, it is imperative to remove the ECG interference from the neuron signals. We first obtain a high spatial density recording using 108 channels. We detect the cardioneural

signals by monitoring the heart rate changes and by observing the symmetry of the neural signals on both sides of the stellate ganglion [20]. We then use Holter to focus on 8 locations for a longer period. We employed ICA to suppress the interference of the ECG signals from the neuron signals.

We perform specific activities that result in changes of heart rate with minimum possible muscle interference. We identify the cardioneural signals based on the heart rate change and the symmetric activity of the stellate ganglion. Since many activities are performed during the recording, signals generated by muscles will also be recorded and mixed with heart and neural signals. Our conjecture is that neural signals concentrate in a small region since the signals are generated by specific nerves, while muscle signals spread among the skin of subjects and therefore affect a larger region of recording channels. This will be our rule of thumb to distinguish these two kinds of signals.

In section 2, we explain the cardioneural signals localization; in section 3, we introduce the application of the ICA method for decomposing the cardioneural signals from ECG signals. In section 4 and 5, we discuss our experiments setup and results, and finally in section 6 we talk about the future direction of our research.

3.2 Exploring Cardioneural location

Jung et al [20] performed continuous 24-hour left stellate ganglion nerve activity (SGNA) and bilateral SGNA recordings in normal ambulatory dogs using implanted electrodes. SGNA was followed immediately by heart rate and blood pressure changes. The experimental results show that the heart rate correlated significantly with SGNA. When there was a sudden increase of SGNA, the sudden increase occurred bilaterally in 90% of the episodes. Their study motivates us to investigate cardioneural signals on human subjects non-invasively. One advantage of the human subject is the ability of the subject to perform special actions. The subject performs various activities which are discussed in details in section 3. We conduct experiments using both high-density electrodes and portable Holter. Our conjecture is that cardioneural signals is seen on certain channels followed immediately by the heart rate changes. Also, symmetric SGNA activity is observed

specifically in our Holter experiments which is another indicator for cardioneural signals.

3.3 ICA for cardioneural signal decomposition

We employ Independent Component Analysis (ICA) to decompose the ECG and neural signals sources. ICA is a family of the related algorithms that performs blind source separation. ICA has been used in biomedical research on many different types of biomedical signals such as Electrocardiogram (ECG), electroencephalogram (EEG), MEG (magnetic counterpart to EEG) and functional magnetic resonance imaging (fMRI) [22]. In the study of biomedical signals *Jung* et al [22] illustrate that, even though, biomedical signals provide detailed information about the physiological process, they are often contaminated by distortions caused by small movement of the electrical contacts know as artifacts. He's [12] work shows that ICA is a powerful technique for noise and artifact removals from the ECG recording.

Assume that our recorded ECG and neural signals, $x = \{x_1(t), ..., x_N(t)\}$, in the time domain are linear mixture of underlying source components $s = \{s_1(t), ..., s_N(t)\}$, i.e., $x = A \cdot u$, where A is an square matrix called mixing matrix [16]. The ICA algorithms decompose the source components which include heart and neural signals respectively, with the key assumption that these components are statistically independent.

In other words, the objective of ICA is to recover another vector u which is equivalent to the original source s subject to permutation and scaling, such that which is obtained by finding a square matrix w. is usually called unmixing matrix. Statistically independence of sources will require the joint probability density function (pdf) of the output sources to be the product of each source pdf.

In our experiment, we apply *"infomax"* ICA algorithm with nature gradient [18], one of a family of algorithms that exploits temporal independence to perform blind separation [16].

3.4 Experiments

We use 108 channel measurements to record high resolution ECG and 8 channel measurements for a longer period. The signals are analyzed with ICA. We test different electrode positions and successfully decompose the ECG and neural sources using ICA.

3.4.1 High Density ECG Recording Experiment

We use 108 channels on the subject's neck, chest and back (Figure 3.1 and 3.2) to perform a high density ECG recording. The setup follows the noninvasive measurement in chapter 2. The cable set consists of 128 pin-type electrodes. In our experiments, we use 113 electrodes with 108 for signals, two for virtual ground at the right side of the waist, and three for further references at left hand and right hand and left foot. The sampling rate is 2048 points per second. The 108 electrodes are attached as follows (Figure 3.1 and 3.2):

- 3 rows of 10 electrodes which are distributed uniformly around the neck.
- 5 rows of 6 electrodes on the chest.
- 8 rows of 6 electrodes on the back where the central three columns are on the spine, next to the left and next to the right of the spine.

The subject performs cardioneural activities while remains still standing. The electrodes are connected to the skin with adhesive pads and electrode gel. In the beginning, the subject breathes normally to set the baseline of the heart rate. Next, the subject performs the Valsalva maneuver. The subject holds breath and plugs nose and mouth while exhales forcibly. The maneuver causes the heart rate changes, thus enables us to capture cardioneural signals. The subject repeats the Valsalva maneuver several times. Finally, the subject drinks a cup of coffee. Immediately after the drink, we observe the heart rate increases.

The 108 channel experiment requires connected cables and instruments which physically limit the activities and the recording period.

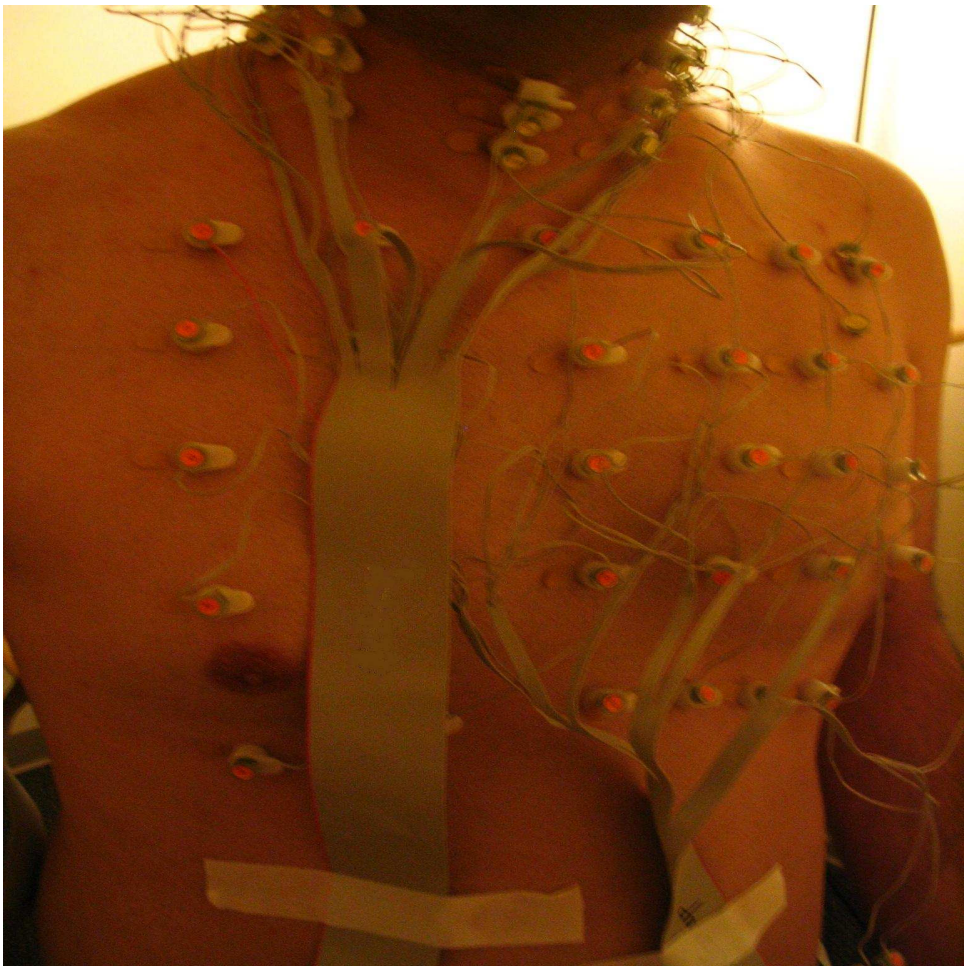

Figure 3.1: High Density 108 channels subject chest experiment setup

3.4.2 Activities and Procedure

We perform various experiments and try several combinations of electrode positions on the subject's chest, back, neck and spine in order to record a relatively strong ECG and neural signals from sympathetic and parasympathetic nervous system. Nevertheless, we might have muscle signals in addition to the cardioneural signals. We dedicate one electrode to monitoring the heart activities and place it on the left side of the chest close to heart.

Each experiment takes 2 hours.The subject performs the following activities during each experiment:

- During the first few minutes, the subject stands still and breathes normally.

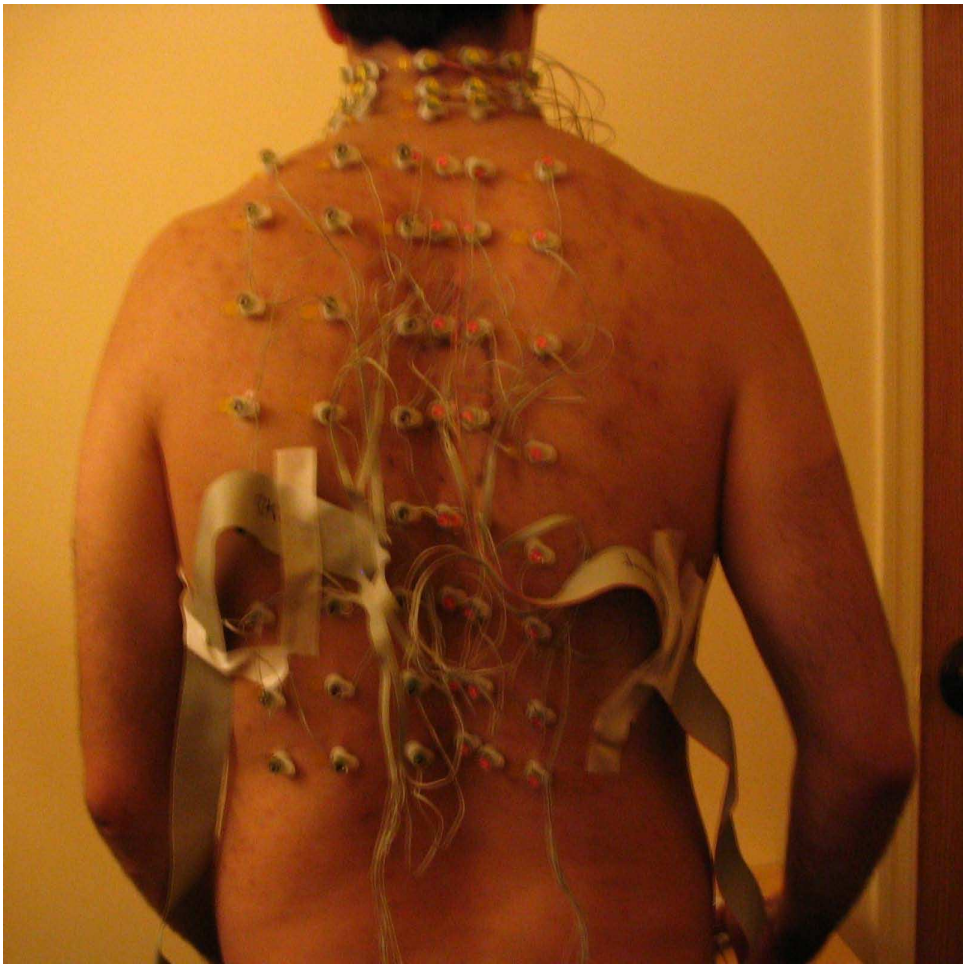

Figure 3.2: High Density 108 channels subject back experiment setup

The record provides the baseline heart rate for comparison.

- The subject performs Valsalva maneuver, which consists of forcibly exhaling against plugged nose and closed mouth, thus forcing air into the middle ear.
- The subject drinks a cup of coffee.
- The subject watches video tapes including comedy, horror movies, and soccer games to stimulate excitement. The heart rate changes in the period.
- The subject performs mathematical calculation to subtract 7 from a number starting at 1000 repeatedly.

During most of the activities the subject keeps sedentary and the average heart rate is close to the baseline.

We devise the activities to excite the cardioneural signals. For Valsalva maneuver, we expect that the sympathetic and parasympathetic neural signals change the heart rate. Valsalva maneuver [34] has four phases. During phase I, blood pressure rises and heart rate decreases due to compression of the aorta and the propulsion of blood into the peripheral circulation. The response is mainly caused by mechanical factors and is not neural mediated. In the following phases, the blood pressure changes and excites the cadioneural signals. The signals alter the heart rate which in turn causes the blood pressure variations, however, with latency. The delay of the blood pressure response creates the heart rate oscillation between bradycardia and tachycardia. We expect that after phase I, the heart rate increases by the sympathetic nervous system and decreases by the vagus nerve.

For a drink of coffee, the subject is affected by the caffeine. The hot temperature of the drink can also stimulate the neural signals. For the video watching and mathematical calculation, the subject goes through mental activities which can also excite the cardioneural signals.

3.5 Results and Analysis

For 108 channel experiment, figure 3 illustrates the result of the mixture signals. The ICA algorithm is applied to mixture of neural signals and ECG recorded by 108 channels (Figures 3.3 and 3.4) in order to decompose the source components of the neural signals and ECG.

The subject starts the Valsava maneuver at 15 second. The maneuver creates heart rate oscillation. In Figures 3.3 and 3.4, starting at 51 second, the heart rate increases from 67 to 86 beats per minute. We observe electrical activities on channels 38 and 39 which coincide with the heart rate changes. Channels 38 and 39 locate on the right side of the thoracic spine (Figure 3.1 and 3.2). We conclude that these signals could be cardioneural and not muscle signals. For High density experiments, we choose the pattern of Figures 3.2 and 3.1. 40 electrodes on and surrounding the thoracic spine (T1 to T5). Thirty electrodes are connected

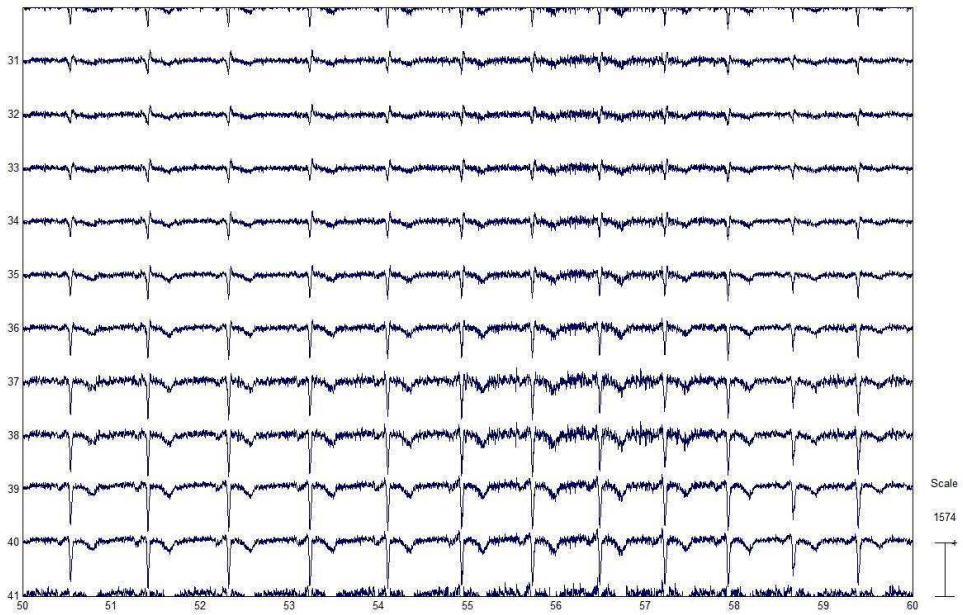

Figure 3.3: Mixture of neural and ECG signals from 108 channel

to the neck and one set on the subject the chest. We see that the heart rate starts changing form 67 to 90 beats per second. The increase in the heart rate coincides with the symmetric electrical activities of the electrodes around the spine (Figure 3.2). We focus on the regions with more signaling activities in the Holter experiment. We are able to explore the cardioneural for a longer period during the Holter experiments and as a result we see more variations in the recorded signals [36].

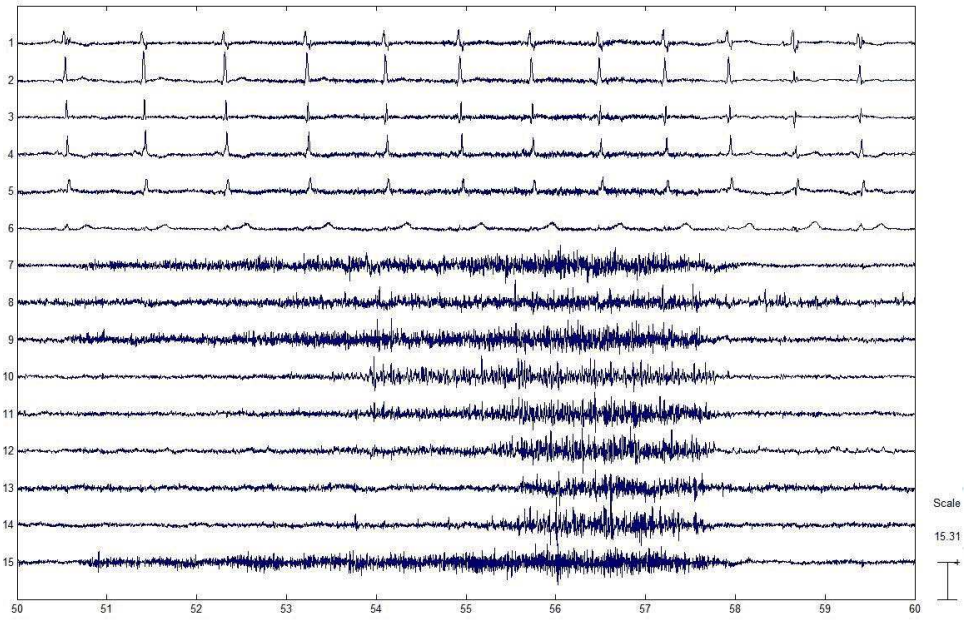

Figure 3.4: ICA decomposed neural and ECG signals from 108 channels

4

Holter Experiment

4.1 Holter Experiment Setup

We use an 8-channel Holter to record both ECG and neural signals. The Holter monitor is a portable device for continuous monitoring. We use an 8-channel Holter 4.1 from Biomedical Instrument Co., Ltd called BI 9800 (http://www.bi-biomed.com). The following is the list of the required equipments to perform the experiment:

- BI 9800 8-channel Holter recorder
- Patient cable integrated with 10 leads wire
- 10 silver-silver chloride disposable pre-jelled electrodes
- 256 MB PCMCIA flash memory card

The Holter is attached to a 10-lead electrode cable. We use the eighth and tenth electrodes as reference and the rest for signals. By convention, the Holter converts the sensed signals to standard 12-lead ECG. We reverse the process to retrieve the original raw data. Pre-jelled disposable electrodes are used to connect the cable. The sampling rate of the Holter is 128 points per second. We use EEGLAB package [11] to visualize the recorded signals.

Figure 4.1: 10 channels Holter

4.2 Holter Experiment Procedure

We perform various experiments and try several combinations of electrode positions on the subject's chest, back, neck and spine in order to record a relatively strong ECG and neural signals from sympathetic and parasympathetic nervous system. Nevertheless, we might have muscle signals in addition to the cardioneural signals.

In our experiment, the reference nodes, electrodes 8 and 10, are connected to the left side of the waist. We dedicate one electrode to monitoring the heart activities and place it on the left side of the chest close to heart. The subject carries the Holter on the belt (Figures 4.2 and 4.3) . Each experiment takes 2 hours.

- During the first few minutes, the subject stands still and breathes normally. The record provides the baseline heart rate for comparison.
- The subject performs Valsalva maneuver, which consists of forcibly exhaling

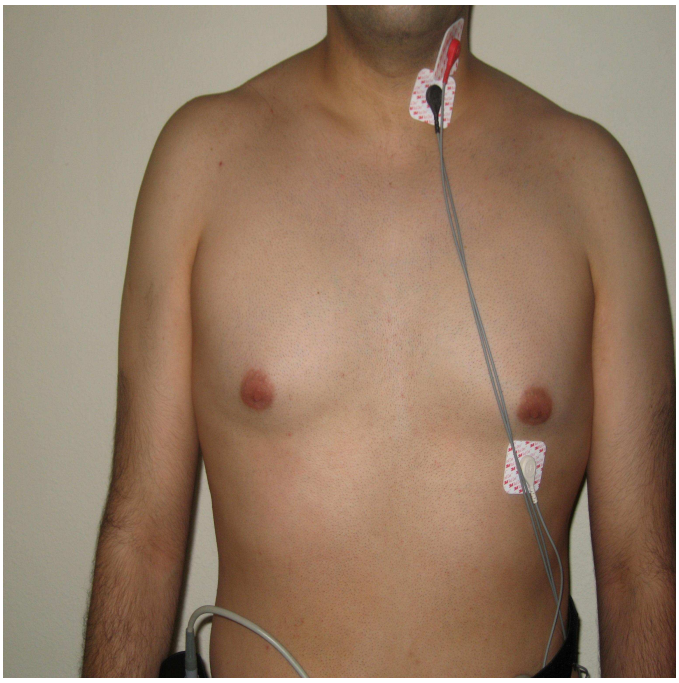

Figure 4.2: Holter chest electrode setup

against plugged nose and closed mouth, thus forcing air into the middle ear.

- The subject drinks a cup of coffee.
- The subject watches video tapes including comedy, horror movies, and soccer games to stimulate excitement. The heart rate changes in the period.
- The subject performs mathematical calculation to subtract 7 from a number starting at 1000 repeatedly.

During most of the activities the subject keeps sedentary and the average heart rate is close to the baseline.

4.3 Results and Analysis

For Holter experiments, we choose the pattern of figure 2. Five electrodes on and surrounding the thoracic spine (T1 to T5). Two electrodes are connected to the left side of the neck and one on to the left side of the chest. Around 2730

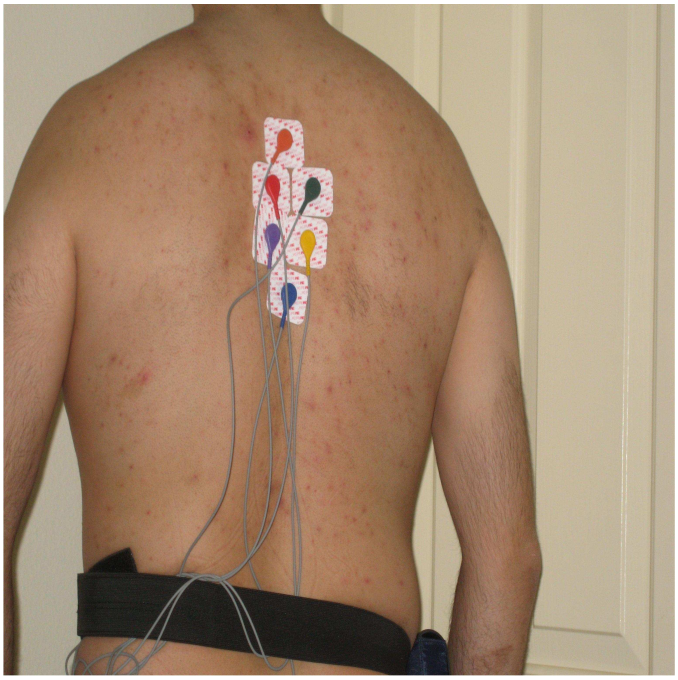

Figure 4.3: Holter back electrode setup

second is when the subject starts drinking coffee. We see that the heart rate starts changing form 86 to 107 beats per second (Figure 4.4 and 4.5). The increase in the heart rate coincides with the symmetric electrical activities of the electrodes around the spine (Figure 4.3). We observe that channels 6 and 7 which are on the left side of the neck for tracking the vagus nerve do not display any specific signaling activity and we interpret the cardioneural signals as sympathetic neuron signals. The subject watches a horror movie starting around 4000 second. In Figure 4.6, the heart rate starts changing at 6409 second. We observe electrical activities on channels 1 and 2 and channels 4 and 5. Note these four channels form a symmetric pattern around the spine. At 6422 (Figure 4.6 and 4.7), the heart rate decrease from 109 to 71 beats per seconds. Here, the electrodes on the neck for tracking the vagus nerve have more signals activity. Also, from the decrease in the heart rate our conclusion is that these could be a possible vagus signals.

Figure 4.6 shows the decomposed signals after ICA extraction. Sources 1 and 2 display ECG signals and sources 3 to 8 display the source components of the neural signals which might include other artifacts.

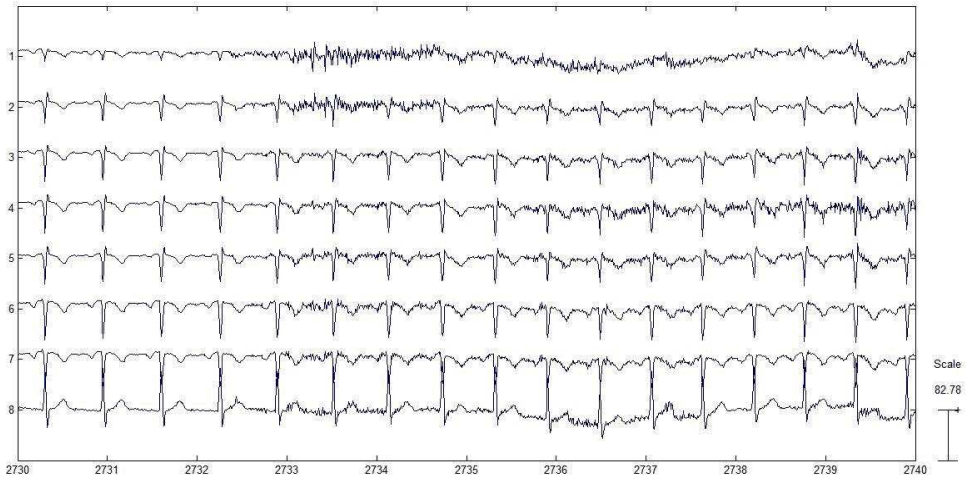

Figure 4.4: Symmetric GNSA mixture signal in the Holter experiment

Around 15427 is when the subject performs the Valsalva maneuver and we see that the heart rate is increased from 73 to 117 beats per second during the Holter experiments (Figure 4.8).

We are able to explore the cardioneural for a longer period during the Holter experiments and as a result we see more variations in the recorded signals.

4.4 Summary and Conclusions

Our method and experimental results show a promising method to extract the neural signals from ECG sources. We localized the cardioneural signals based on the changes in the heart rate and the symmetric SGNA. We applied ICA to decompose the cardioneural signals from the ECG misture.

We get better neural extraction if we place few electrodes on left side of the neck for vagus nerve activity and few electrodes on and around thoracic spine T1 to T5 and cervical spine C5 to C8. Also, we need an additional probe on the left side of the chest in traditional ECG place to keep track of heart activities. The rule of thumb is that while muscle signals affect a higher spatial domain neural signals correspond to specific nerve and concentrated in smaller region.

For future work, our goal is to capture the simultaneous readings of cardioneural signaling with heart rate and blood pressure changes. Also, we would

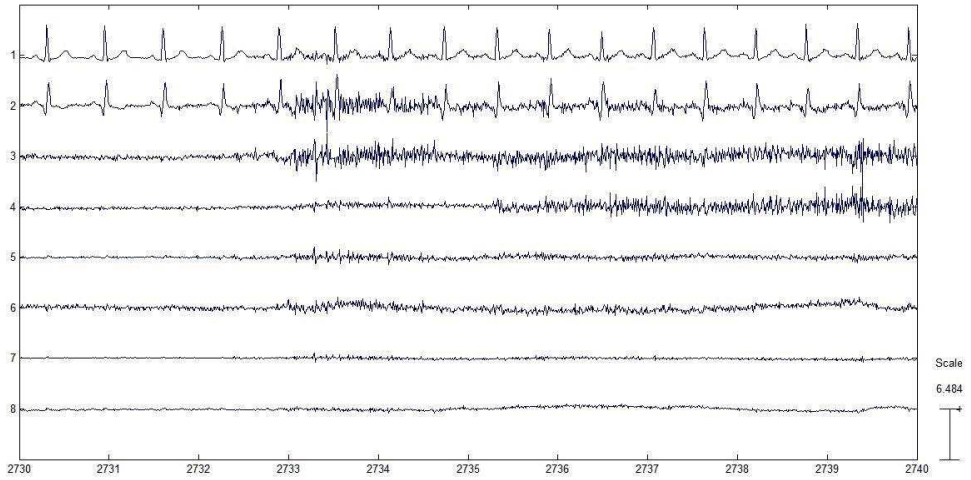

Figure 4.5: ICA extraction of the symmetric GNSA in the Holter experiment

like to establish an invasive recording on the dog model as a baseline neural signals standard, and compare the signal characteristics of this recording in time and frequency domain to the non-invasive extracted neural signals. The ongoing research will require more quantitative measurements. We also need to further differentiate the sources of electrical signaling of the heart and nerves from muscle and other artifacts [36].

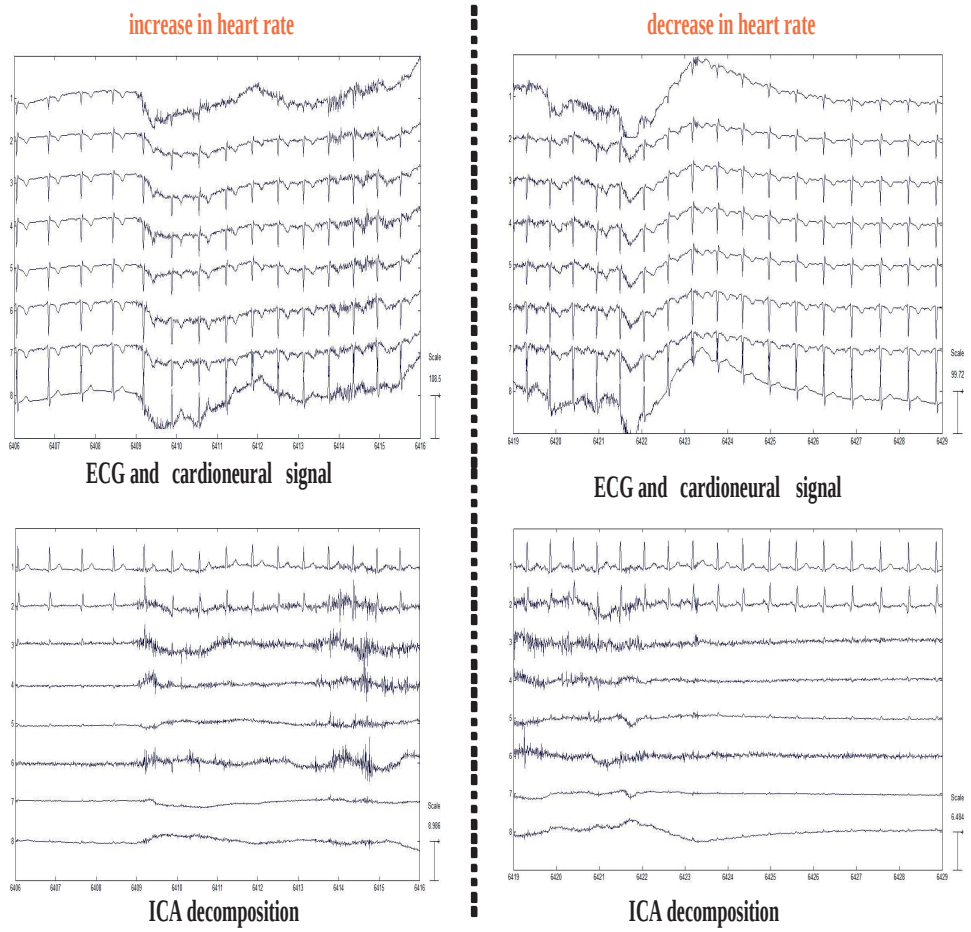

Figure 4.6: Increase and decrease of the heart rate during watching movie in the Holter Experiment

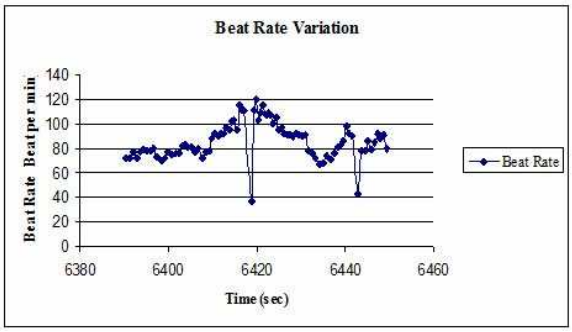

Figure 4.7: Heart beat rate changes during watching movie in the Holter Experiment

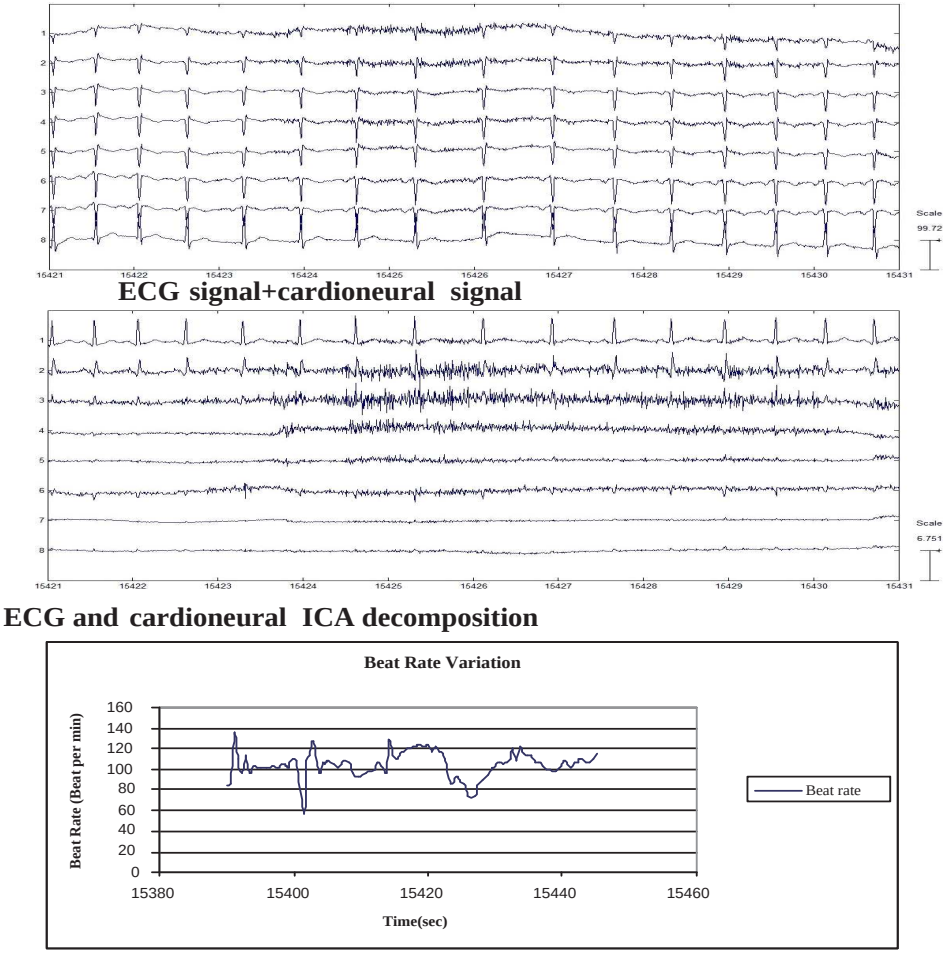

Figure 4.8: Heart rate oscillation in Valsalva maneuver recorded using Holter

5

Conclusions and Future Direction

According to American Heart Association heart diseases are America's number one killer. Cardioneural signal influence heart activities and rhythms. Damage to nerves extrinsic to the heart, such as the stellate ganglia, as well as to intrinsic cardiac nerves from diseases that may affect nerves primarily, such as viral infections, or secondarily, from the disease that cause cardiac damage, may produce cardio neuropathy. Also, the nerve fiber density and regional sympathetic hyperinnervation in the ventricles is correlated with the occurrence of spontaneous ventricular tachyarrythmia or Sudden Cardiac Death. In this work we proposed a comprehensive study for exploring and analyzing cardioneural signal to track, monitor and potentially prevent heart arrhythmias.

In our current study, we explored the cardioneural signal from noninvasive measurements. Previously, Jung et al [19]. performed an invasive nerve study for monitoring the circadiane nerve activities in ambulatory dogs. Their study results motivated us, to develop an original research for exploring the cardioneural signal on human subjects. Hence, we performed both high density and portable noninvasive measurements to extract the cardioneural signal. We tried different combinations of the activities and location to probe the cardioneural signal based on the heart rate variation. We applied ICA algorithm to decompose the cardioneural signal from mixture of ECG measurements. The qualitative promising results demonstrate the feasibility of this direction.

First, we focus on extracting the cardioneural signal with robustness and

high fidelity. The current research could be continued with more high density noninvasive measurements to gain comprehensive knowledge about the exact locations for probing the cardioneural signal. We use high density electrodes, i.e. more than 100, on potential locations on the subject surface such as neck, chest, front and sides. We will monitor not only changes in heart rate, but also blood pressure as well as the cardioneural signal. We will apply different mathematical source separation algorithms to extract the cardioneural signal from the mixed signal measurement and finally choose the proper method.

The future direction is to develop hardware and software for monitoring cardioneural signal that eventually can save lives at the moments when the heart arrhythmias happen by calling 911 or interacting with subject pacemaker or implantable defibrillator. For a more detailed study simultaneous study and analysis of cardioneural signal and other biomedical signals such as EEG, MEG, ECG and fMRI would be beneficial.

The next step is to establish a baseline neural signal as a standard, and then compare the signal characteristics of this recording i.e. in time and frequency domain, to the extracted neural signals. In previous research, we qualitatively demonstrated the extracted neuron signal. However in order to differentiate noise from the cardionerual signal quantitative measurement and analysis is required in our research plan. We plan to perform simultaneous skin electrode recording and stellate ganglion recording, and correlate the two.

For independent validation, we need to make certain synthetic mixture of neural signals and ECGs, and then use the proposed method to decouple neural signals from ECG, this provides a way to evaluate and choose or derive the suitable decomposition algorithm. For the baseline or neural signal, we will utilize the invasive neural measurements from dog or possible sources. Following extensive and fine grain measurements and deriving the exact path of the cardioneural signal, we need to precisely try proper strategies for artifact and noise mitigation.

For next step, it would be beneficial to verify our noninvasive model against measurements and utilize suitable source localization methods for deriving cardioneural signal source path. The development of appropriate mathematical and physical simulation models that reflect cardioneural signal propagation and dis-

tortion through different human subject membrane from the neuron source to the probing electrodes is necessarily for cardioneural monitoring. We need to derive the minimum possible electrode numbers and exact locations which we can exploit in our invasive and noninvasive cardioneural tracking. This is crucial for next stage of the proposed plan which is designing a portable cardioneural measurement device. We will derive the methodology to measure the quantitative characteristic of the cardioneural signal such as current, voltage, etc. This future direction of this study will also cover simultaneous study and analysis of the cardioneural signal and different types of biomedical signals such as electroencephalogram (EEG), ECG, MEG and functional magnetic resonance imaging (fMRI). Our forecast is that we will acquire valuable results from these simultaneous experiments which guide us along the course of the project.

Our mission aims to detect and intervene in life danger situations. The goal is to track cardioneural signal and alert heart arrhythmias in human subjects. The technology we prospect to design for cardioneural signal would be such that can possibly intervene in threatening situations with proper diagnosis and therapy steps like injecting proper medicine, calling 911, sending special signal or alert. It could be synchronized or in communication with subject or patients pacemaker or implantable defibrillator. Our plan in this research is to design the portable cardioneural signal monitoring device with wireless facilities. This research plan would be a novel cardioneural monitoring technology which will be beneficial for diagnosis heart arrhythmias and could save human lives in case of possible threatening or cardiac arrest.

Bibliography

[1] A. K. Barros, A. Mansour, and N. Ohnishi. Removing artefacts from electrocardiographic signals using independent component analysis. *Neurocomputing*, 22:173–186, 1998.

[2] D. H. Bennett. Cardiac arrhythmias: Practical notes on interpretation and treatment. *Hodder Arnold Publication*, 2007.

[3] E. Braunwald, D. P. Zipes, P. Libby, and R. Bonow. Braunwald's heart disease: A textbook of cardiovascular medicine. *ELSEVIER SAUNDERS, 7th REV.*, 2005.

[4] J. Cao, L. Chen, P. Wolf, T. Ohara, M. Lee, B. KenKnight, H. Karagueuzian, M. Fishbein, and P. Chen. Nerve sprouting and sudden cardiac death. *Circulation Research*, pages 816–821, 2000.

[5] J. Cao, M. Fishbein, J. Han, W. Lai, T. Wu, L. Czer, P. Wolf, T. Denton, I. Shintaku, P. Chen, and L. Chen. Relationship between regional ventricular hyperinnervation and ventricular arrhythmia. *Circulation Research*, pages 1960 – 1969, 2000.

[6] J. Cardoso. High-order contrasts for independent component analysis. *Neurocomputing*, pages 1:157–192, 1999.

[7] J. Cardoso and A. Soloumiac. Blind beamforming for non-gaussian signals. *IEE Proceedings*, 140(46):362–370, 1993.

[8] F. Castells, P. Laguna, L. Sornmo, A. Bollmann, and J. M. Roig. Principal component analysis in ECG signal processing. *EURASIP Journal on Advances in Signal Processing*, 2007:Article ID 74580, 21 pages, 2007.

[9] F. Castells, J. J. Rieta, J. Millet, and V. Zarzoso. Spatiotemporal blind source separation approach to atrial activity estimation in atrial tachyarrhythmias. *IEEE Transactions on Biomedical Engineering*, 52(2):258–267, February 2005.

[10] P. Comon. Independent component analysis, a new concept? *Signal Processing*, 36:287–314, 1994.

[11] E. Delorme and S. Makeig. EEGLAB: an open source toolbox for analysis of single-trial eeg dynamics. *Journal of Neuroscience Methods*, pages 134:9–21, 2004.

[12] T. He, G. Clifford, and L. Tarassenko. Application of ICA in removing artefacts from the ECG. *Neuro Computing and Applications*, 12, 2002.

[13] T. He, G. Clifford, and L. Tarassenko. Application of independent component analysis in removing artefacts from the electrocardiogram. *Neuro Computing and Applications*, 15(2), 2006.

[14] H. Hnninen, P. Takala, M. Mkijrvi, P. Korhonen, L. Oikarinen, K. Simelius, J. Nenonen, T. Katila, and L. Toivonen. ST-segment level and slope in exercise-induced myocardial ischemia evaluated with body surface potential mapping. *The American Journal of Cardiology*, 88:1152–1156, 2001.

[15] H. Hnninen, P. Takala, J. Rantonen, M. Mkijrvi, K. Virtanen, J. Nenonen, T. Katila, and L. Toivonen. ST-T integral and T-wave amplitude in detection of exercise-induced myocardial ischemia evaluated with body surface potential mapping. *J of Electrocardiology*, 36:89–98, 2004.

[16] A. Hyvaerinen. Survey on independent component analysis. *Neural Computation Survey*, 2:94–128, 1999.

[17] A. Hyvarinen, J. Karhunen, and E. Oja. Independent component analysis. *John Wiley & Sons*, 2001.

[18] S. ichi Amari. Natural gradient works efficiently in learning. *Neural Computation*, 10:251–276, 1998.

[19] B. Jung, D. AS, T. AY, G. G, Z. S, W. DC, A. AG, F. GA, M. C, L. SF, C. LS, and C. PS. Circadian variations of stellate ganglion nerve activity in ambulatory dogs. *Heart Rhythm*, 2006.

[20] B. Jung, A. Dave, A. Tan, G. Gholmieh, S. Zhou, D. Wang, A. Akingba, G. Fishbein, C. Montemagno, S. Lin, L. Chen, and P. Chen. circadian variations of stellate ganglion nerve activity in ambulatory dogs. *Heart Rhythm*, 3:78–85, 2005.

[21] T. Jung, C. Humphries, T. Lee, M. McKeown, V. Iragui, S. Makeig, and T. Sejnowski. Removing electroencephalographic artifacts from by blind source separation. *Psychophysiology*, pages 163–178, 2000.

[22] T. Jung, S. Makeig, T. Lee, M. Mckeown, G. Brown, A. Bell, and T. Sejnowski. Independent component analysis of biomedical signals. In *2nd International Workshop on Independent Component Analysis and Signal Separation*, 2000.

[23] T. Jung, S. Makeig, M. Mackeown, A. Bell, T. Lee, and T. Sejnowski. Imaging brain dynamics using independent component analysis. *Proceedings of The IEEE*, 89(7), 2001.

[24] L. D. Lathauwer, D. Callaerts, B. D. Moor, and J. Vandewalle. Fetal electrocardiogram extraction by source subspace separation. In *Proocedings of IEEE/ATHOS Signal Processing Conference on High-Order Statistics*, pages 134–138, 1995.

[25] L. D. Lathauwer, B. D. Moor, and J. Vandewalle. Fetal electrocardiogram extraction by blind source subspace saparation. *IEEE Transactions on Biomedical Engineering*, 47:567–572, 2000.

[26] T. Lee, M. Girolami, A. Bell, and T. Sejnowski. A unifying information-theoretic framework for independent component analysis. *Computers and Mathematics with Applications*, 39:1–21, 2000.

[27] G. Li and B. He. Localization of the site of origin of cardiac activation by means of a heart-model-based electrocardiographic imaging approach. *IEEE Transactions on Biomedical Engineering*, 48(9):660–669, June 2001.

[28] G. Li, X. Zhang, J. Lian, and B. He. Noninvasive localization of the site of origin of paced cardiac activation in human by means of a 3-D heart model. *IEEE Transactions on Biomedical Engineering*, 50(9):1117–1120, September 2003.

[29] S. Makeig, T. Jung, A. Bell, D. Ghahremani, and T. Sejnowski. Blind separation of auditory event-related brain responses into independent component analysis. *Proceeding of National Academy of Science USA*, 94:10979–10984, 1997.

[30] J. A. Nelder and R. Mead. A simplex method for function minimization. *Computer Journal*, 7, 1965.

[31] K. Park, J. Lee, and K. Lee. ECG signal processing using basis function of independent component analysis. In *Proceeding (458) Biomedical Engineering*, pages 425–429, 2005.

[32] C. Ramanathan, R. Ghanem, P. Jia, K. Ryu, and Y. Ruby. Noninvasive electrocardiographic imaging for cardiac electrophysiology and arrhythmia. *Nature Publishing Group of Nature Medicine Advance Online Publication*, 2004.

[33] J. Rieta, F. Castells, C. Sanchez, V. Zarzoso, and J. Millet. Atrial activity extraction for atrial fibrillation analysis using blind source separation. *IEEE Transactions on Biomedical Engineering*, 51(7):1176–1186, July 2004.

[34] M. Risk, M. Berghoff, and R. Freeman. Characterization of the valsalva maneuver using wavelet transform. *Computers in Cardiology*, 2000.

[35] R. Sameni, C. Jutten, and M. B. Shamsollahi. What ICA provides for ECG processing: Application to noninvasive fetal ECG extraction. In *IEEE International Symposium on Signal Processing and Information Technology*, pages 656–661, 2006.

[36] A. Shayan, Y. Zhu, Y.-N. Cheng, C.-K. Cheng, S.-F. Lin, and P.-S. Chen. Exploring cardioneural signals from noninvasive ecg measurement. *Bioinformatics and Bioengineering, 2007. BIBE 2007. Proceedings of the 7th IEEE International Conference on*, pages 1134–1138, Oct. 2007.

[37] A. Shayan, Y. Zhu, W. Zhang, T. Jung, J. Duann, S. Makeig, and C. Cheng. Spatial density reduction in the study of ECG signal using independent component analysis. In *Proceedings of 29th Annual Internatinoal Conference of the IEEE Engineering in Medicine and Biology Society*, 2007.

[38] K. Simelius, L. Reinhardt, J. Nenonen, I. Tierala, L. Toivonen, and T. Katila. Self-organizing maps in arrhythmia localization from body surface potential mapping. In *Proceedings of 19th Annual Conference of IEEE / EMBS*, pages 62–64, 1997.

[39] K. Simelius, I. Tierala, T. Jokiniemi, J. Nenonen, L. Toivonen, and T. Katila. A body surface potential mapping system in clinical use. *Medical & Biological Engineering & Computing*, 34(1):107–108, 1996.

[40] S. Tong, A. Bezerianos, and J. P. et al. Removal of ECG interference from the EEG recordings in small animals using independent component analysis. *Journal of Neuroscience Methods*, 108:11–17, 2001.

[41] F. Vrins, V. Vigneron, C. Jutten, and M. Verleysen. Abdominal electrodes analysis by statistical processing for fetal electrocardiogram extraction. In *Proceedings of 2nd IASTED International Conference on Biomedical Engineering*, pages 244–249, February 2004.

[42] B. Widrow, J. R. Glover, J. R. Glover, and J. M. M. et al. Adaptive noise cancelling: Principles and applications. *Proceedings of the IEEE*, 63(12):1962–1976, December 1975.

[43] J. O. Wisbeck, A. K. Barros, and R. Ojeda. Application of ICA in the separation of artefacts in ECG signals. In *Proceedings of International Conference on Neural Information Processing*, 1998.

[44] Y. Zhu, T. L. Chen, W. Zhang, T.-P. Jung, J.-R. Duann, S. Makeig, and C.-K. Cheng. Noninvasive study of the human heart using independent component

analysis. *BioInformatics and BioEngineering, 2006. BIBE 2006. Sixth IEEE Symposium on*, pages 340–347, Oct. 2006.